STOCHASTIC MODELING OF THE VARIATION OF VELOCITY AND PERMEABILITY AS A FUNCTION OF EFFECTIVE PRESSURE USING THE BED-OF-NAILS ASPERITY-DEFORMATION MODEL

A Thesis

by

EZEQUIEL GENOVA BARAZARTE

Submitted to the Office of Graduate Studies of
Texas A&M University
in partial fulfillment of the requirements for the degree of

MASTER OF SCIENCE

August 2007

Major Subject: Geophysics

STOCHASTIC MODELING OF THE VARIATION OF VELOCITY AND PERMEABILITY AS A FUNCTION OF EFFECTIVE PRESSURE USING THE BED-OF-NAILS ASPERITY-DEFORMATION MODEL

A Thesis

by

EZEQUIEL GENOVA BARAZARTE

Submitted to the Office of Graduate Studies of
Texas A&M University
in partial fulfillment of the requirements for the degree of

MASTER OF SCIENCE

Approved by:

Chair of Committee,	Richard L. Carlson
Committee Members,	Anthony F. Gangi
	Thomas A. Blasingame
Head of Department,	John H. Spang

August 2007

Major Subject: Geophysics

ABSTRACT

Stochastic Modeling of the Variation of Velocity and Permeability as a Function of Effective Pressure Using the Bed-of-Nails Asperity-Deformation Model. (August 2007)

Ezequiel Genova Barazarte, B.S., Eckerd College

Chair of Advisory Committee: Dr. Richard Carlson

The mechanical and transport properties of porous and cracked media, such as velocity and permeability, are sensitive to the effects of effective pressure, which itself is a function of the confining pressure and the pore-fluid pressure. The dependence of permeability and velocity on effective pressure has previously been modeled using the Bed-of-Nails asperity-deformation model. The main objective of this research was to explore the sensitivity of the Bed-of-Nails and effective-pressure models to random, Gaussian errors, by using an inverse approach. To achieve this, numerical modeling of pre-existing velocity and permeability experimental data sets was done.

Extrapolation to 600 MPa was performed using an epidosite data set of compressional velocity as a function of confining pressure, only using measurements in the range 0-100 MPa. The results showed that, given sufficient data and considering random error only, extrapolation can be done with a level of error of less than 1.5%. Model error can also be significant in this type of exercise because it can give rise to systematic misfit, although in this case it was shown that the effects of model error were not considerable. Modeling the variation of compressional velocities as a function of

confining and pore-fluid pressures in a deep-sea chalk showed that the best-fitting asperity-deformation model is sensitive to the effective-pressure model.

Measurements of permeability in a Navajo-sandstone specimen as a function of confining pressure were numerically modeled, and the results showed that measurements made at low pressures, specifically near $P_e = 0$, are very important to constrain the model. The same result was found in the case of permeability as a function of confining and pore-fluid pressure in a Wilcox-shale where the lack of measurements near $P_e = 0$ caused the error in the model parameters to be overestimated. This occurs because the rate of change of permeability as a function of effective pressure is very high at low pressures. The lack of sufficient data near $P_e = 0$ overestimates the curvature matrix and, therefore, the errors in the model parameters.

DEDICATION

To my parents

ACKNOWLEDGMENTS

I would like to thank my committee chair, Dr. Carlson, for all the time he put into this project on a weekly basis. I also want to thank him for his guidance and support during my studies at Texas A&M University. I would also like to thank my other committee members, Dr. Gangi and Dr. Blasingame, for their support and help with this research.

Thanks to my parents because they have supported and helped me in all stages of my education. Finally, I would like to thank my wife, Laura, for being there for me when I have needed her and for her support and advice.

TABLE OF CONTENTS

LIST OF FIGURES

FIGURE Page

LIST OF TABLES

CHAPTER I

INTRODUCTION

The properties of porous and cracked media depend on both the confining pressure, P_c, and the pore-fluid pressure, P_p. Consider a property M of a porous solid, such as velocity or permeability, that is a function of P_c and P_p

$$M = M(P_c, P_p) \tag{1}$$

Measurements made at $P_p = 0$ will yield a function

$$M = M(P_c, 0) \tag{2}$$

If the pore-fluid pressure is no longer zero, the effective pressure P_e is defined as that combination of confining and pore-fluid pressures that has the same effect on the property M as when the pore-fluid pressure is zero [*Robin*, 1973]

$$M(P_e) = M(P_c, P_p) = M(P_c, 0) \tag{3}$$

The concept of effective pressure is very important for characterizing the mechanical and transport properties of fractured and porous rocks [*Terzaghi*, 1936; *Hubbert and Rubey*, 1959].

There is no single effective-pressure law that applies to all properties [*Robin*, 1973]. Even measurements of the same property in different samples can reflect different effective-pressure relationships depending on the number of parameters that can be

---

This thesis follows the style of *Journal of Geophysical Research*.

resolved from the data. The precision of the measurements will dictate whether we can apply a particular expression, or if one can use a simpler expression with fewer parameters.

Because the effective pressure equals the confining pressure for $P_p = 0$ and the effect of pore pressure is observed to vary with P_c and P_p, effective-pressure laws can be written as

$$P_e = P_e(P_c, P_p) = P_c - \chi(P_e)P_p \tag{4}$$

Gangi and Carlson [1996] noted that P_e has been given various approximations,

$$P_{e1} \equiv P_d \equiv P_c - P_p \tag{5}$$

$$P_{e2} = P_c - \chi P_p \qquad 0 \le \chi \le 1 \tag{6}$$

$$P_{e3} = P_c - (\chi_o - aP_d)P_p \tag{7}$$

where χ, χ_o, a are constants. Which of these approximations applies to a particular data set depends on a number of considerations including: 1) the nature of the medium, 2) the range of P_c and P_p over which measurements are made, 3) measurements made at low pressures and, 4) the precision of the measurements. Notice that each succeeding approximation incorporates more parameters. The precision of measured values affects the resolution of the parameters (χ , χ_o , a) from experimental data.

Inverse methods are commonly used in the geosciences to estimate model parameters from experimental data; however, the estimated parameter values have uncertainties even for the case when the model is correct because of the errors in the experimental data. The range of the data can also affect the resolution of the model parameters. A

good example illustrating this point comes from *Carlson and Gangi* [1985], who concluded that both low pressure (*e.g.*, less than 10 MPa) and high pressure (*e.g.*, greater than 1000 MPa) data were needed to define both the properties of the cracks and the grains from the variation of velocity with pressure. *Christensen* [1974] addressed a similar issue for mafic and ultramafic rocks.

Random errors also affect the estimation and resolution of model parameters. Uncertainties depend on the errors (noise) in the measurements and, therefore, our ability to resolve specific model parameters depends directly on the noise in the data. For example, let us say that P_{e3} (equation (7)) is the most appropriate approximation for the property of a particular rock, but due to the scatter in the data it might be possible to resolve or constrain χ but not the parameter a (*i.e.*, the results show a is not significantly different from zero, where a is the estimate of the parameter obtained from the fit). In this case, the choice of models that can be resolved from the data would be limited to P_{e2} (equation (6)).

The main objective of this study is to assess the resolution of the effective pressure and the "Bed-of-Nails" asperity-deformation [*Gangi*, 1975, 1978] model parameters based on four experimental data sets [*Nelson*, 1975; *Carlson and Gangi*, 1985; *Gangi and Carlson*, 1996; *Kwon et al.*, 2001], and explore various aspects of fitting a non-linear model to compressional velocity and permeability data. These various aspects include the fact that the resolution of the model parameters depends on the level of error present in the data and, therefore, the ability to constrain the model.

A compressional-velocity data set as a function of confining pressure [*Carlson and Gangi*, 1985] was used and two main issues were addressed; the first one was the sensitivity of the Bed-of-Nails model parameters to the level of error in the data, and the fact that the error in the model parameters was proportional to the error present in the data. The second issue we addressed here was extrapolation up to 600 MPa from measurements made between 0-100 MPa, where the parameter P_i was the most sensitive to constrain due to lack of measurements at "negative" pressures. Extrapolating data is often considered bad practice, but it can be justified if the fit is made based on a theoretical model that explains the data well enough [*e.g.*, *LuValle*, 2004]. High-pressure values are often difficult and costly to make. The ability to extrapolate high-pressure measurements from those made at low pressures is, therefore, worth studying since it can greatly improve the efficiency of the experiment.

A chalk data set [*Gangi and Carlson*, 1996] of compressional velocities as a function of both confining and pore-fluid pressures was used to explore the various effective-pressure approximations given in (5-7) using the Bed-of-Nails asperity-deformation model [*Gangi*, 1975, 1978]. A unique feature of this process is that there is a model within a model: 1) velocity as a function of effective pressure, and 2) effective-pressure as a function of confining pressure and pore-fluid pressure. The important result here is that the ability to constrain the various effective-pressure models is conditioned by the resolution of one single parameter, P_i. We find that the various P_e models are still resolved at high levels of error.

Permeability measured as a function of confining pressure in a Navajo-sandstone sample [*Nelson*, 1975] was used to explore the sensitivity of the Bed-of-Nails model to the level of error present in the measured permeabilities. The most important result is that having a measurement at $P_c = 0$ determines the precision of the Bed-of-Nails-model parameters.

Permeability in a Wilcox shale [*Kwon et al*., 2001], measured as a function of both confining and pore-fluid pressure, was used to explore the differences of using a non-linear fitting routine compared to the linearized version used by *Kwon et al*. [2001] to resolve the data. Another issue here was the fact that removing the measurement at $P_e = 0$ caused the error space to change significantly and, therefore, limited the ability to constrain the Bed-of-Nails-model parameters.

Each experimental data set has been fitted using the Bed-of-Nails asperity-deformation model [*Gangi*, 1975, 1978], and the results have been used to generate synthetic data sets to which Gaussian errors have been added. These numerical experiments are designed to better understand the specific issues previously mentioned, so that they can be addressed in a way that is statistically meaningful. By generating synthetic data sets, we can also assess the validity of the various experimental data sets, and whether the results are typical for such experiments.

CHAPTER II

BACKGROUND

In this section, we discuss the concept of effective pressure in more detail and how effective-pressure laws can be derived using general asperity-deformation models, which explain the variation of mechanical and/or transport properties as a function of pressure. In the Bed-of-Nails asperity-deformation model [*Gangi*, 1975, 1978] effective pressure depends on the fractional area of contact of the asperities of a crack in a rock [*Gangi and Carlson*, 1996].

Asperity-Deformation Model

Asperity-deformation models are used to obtain effective-pressure laws that describe the variation of mechanical and/or transport properties as a function of pressure [*Gangi*, 1978]. *Gangi and Carlson* [1996] derived an asperity-deformation model for effective pressure from force-balance equations based on P_c, P_p and the load supported by the asperities, which they called an "asperity pressure", P_a. They found this effective pressure to depend on the fractional area of asperity contact, A_f. When confining pressure P_c is applied to a rock, cracks close, and more asperities come into contact. In the force-balance equation the externally-applied force, F_c (P_c), is balanced by the sum of the pore-fluid-pressure force F_p (P_p) and by the force acting on the asperities in contact, F_a (P_a).

$$F_c = AP_c = AP_a + (A - A_c)P_p = F_a + F_p \tag{8}$$

where

A = area of crack

A_c = area of asperity contact

$P_a = F_a/A$ = "asperity pressure", and $P_a \cong P_e$

Rearranging equation (8), the effective pressure is given by

$$P_e(P_c, P_p) = P_a = P_c - (1 - A_f)P_p \tag{9}$$

where $A_f = A_c/A$ is defined as the fractional area of contact and is itself a function of the "asperity pressure", P_a

$$A_f = A_f(P_e) \approx A_f(P_a) \tag{10}$$

if $P_e \sim P_d$, where P_d is the differential pressure, and $P_c > P_p$ [*Gangi and Carlson*, 1996]. This assumes χ or $(\chi_o - aP_d) \sim 1$ (equations (6-7)). Thus

$$P_e \cong P_c - (1 - A_f(P_d))P_p \tag{11}$$

If we allow for some fractional area of contact A_{fo} at zero effective (or differential) pressure, $A_f(0) = A_{fo}$, then

$$A_f(P_e) \approx A_{fo} + \frac{\partial A_f}{\partial P_d} P_d \tag{12}$$

and

$$P_e = P_c - (1 - A_{fo} - \frac{\partial A_f}{\partial P_d} P_d)P_p \tag{13}$$

Equation (13) is equivalent to the definition of P_{e3}, with $\chi_o = 1 - A_{fo}$, and $a = \partial A_f / \partial P_d$.

Effective Pressure

The effective pressure depends on how the external load is distributed between the asperities and the pore fluid. The effective pressure depends directly on the fractional area of contact, A_f (equation (13)). *Gangi and Carlson* [1996] summarized several

approximations of effective pressure, the simplest case being where P_e equals the differential pressure P_d [*e.g.*, *Terzaghi*, 1936; *Handin*, 1958; *Hubbert and Rubey*, 1959] given in (5). This approximation is accurate when the material is very "friable" (*i.e.*, with small areas of contact of asperities such as in soils, or rocks near fracture), and $A_f \sim 0$. In noisy data sets where the scatter is significant, this definition can be a good approximation because it may not be possible to resolve more model parameters (*e.g.*, χ_o, a).

The second approximation, P_{e2}, given in (6), assumes χ to be a positive constant, generally less than or equal to one [*e.g.*, *Nur and Byerlee*, 1971; *Todd and Simmons*, 1972; *Walsh*, 1981]. This means that A_f is constant. χ depends on the nature of the material (*e.g.*, well-cemented rocks and porous rocks), but the precision of measurements may also be a factor in defining the value of the constant χ. For example, *Kwon et al*. [2001] found the effective-pressure coefficient estimate χ to be 0.99 ± 0.06 for Wilcox shale when measuring permeability. Even though the permeability in this case depends on both P_c and P_p, the value of χ is clearly indistinguishable from one and, therefore, the data are consistent with $P_e = P_d$.

The third approximation of effective pressure is given by (7). In this case, the coefficient, $\chi = \chi_o - aP_d$, is itself a function of the pressures [*e.g.*, *Nur and Byerlee*, 1971; *Todd and Simmons*, 1972; *Robin*, 1973, *Gangi and Carlson*, 1986] yielding two model parameters (*i.e.*, χ_o and *a*). The fractional area of contact, A_f, is a linear function of P_d for this case. Applying this approximation to measurements of P-wave velocity in

a sample of deep-sea chalk, *Gangi and Carlson* [1996] found χ_o ~ 0.93 and a ~ 0.014 MPa^{-1}. Though they did not report the uncertainties in these parameters, this data set is useful for exploring the effect of experimental error on the resolution of the model parameters.

Bed-of-Nails Asperity-Deformation Model

The advantages of using the Bed-of-Nails model are its simplicity and its flexibility. It also has excellent application to various velocity and permeability data sets [*e.g.*, *Nelson*, 1975; *Ciampa*, 1980; *Kwon et al*., 2001]. In the model, asperities are treated as a distribution of rods with different heights, which are mechanically equivalent to the ones used in other models in which the asperities are hemispheres, wedges, cones, etc. [*e.g.*, *Greenwood and Williamson*, 1966; *Jones,* 1975; *Walsh and Grosenbaugh*, 1979].

Different height-distribution functions (*e.g.*, exponential, Gaussian, power-law) can be used in the Bed-of-Nails model. *Gangi* [1978] chose to use a power-law form for the height distribution function given by

$$N(h) = N_T (1 - h / w_o)^{n-1} \qquad 1 \le n \le \infty \qquad (14)$$

where *N(h)* is the number of asperities having heights between h and w_o (w_o ~ maximum crack width), and N_T is the total number of rods. This distribution function was chosen because it is easy to integrate and thus gives a simple, but useful analytical expression. The power coefficient n characterizes the distribution function of the asperity lengths [*Gangi*, 1978]. For example, a very smooth surface (*i.e.*, a well-polished surface) with only a very few short asperities is characterized by n~1. On the other hand, a large n

describes a fracture with only a few tall asperities (*e.g.*, a new fracture with just a few large intact asperities).

Velocity depends on the elastic modulus of the cracks, which increase as asperities are compressed, and permeability depends on the width w of the crack, which is a function of effective pressure P_e because the width narrows as the asperities are compressed. For the Bed-of-Nails model, the width w of the crack varies with effective stress P_e [*Gangi,* 1978] as

$$w / w_o = 1 - (P_e / P_1)^{1/n} \tag{15}$$

where

$P_1 = EN_o w_o{}^2 b / n =$ constant

E = the rod's Young's Modulus

N_o = average number of rods per unit area

b = the ratio of the rod's cross-sectional area to their length (assumed equal for all rods)

P_1 is a constant proportional to E, which varies from rock to rock [*Gangi,* 1978, 1981].

The pressure dependence of the permeability k can then be explained by this model because k is proportional to w^3, that is

$$k = k_o \left(\frac{w}{w_o} \right)^3 \tag{16}$$

where k_o is the permeability when $w = w_o$. The pressure dependence of permeability is thus

$$k(P_e) = k_o [1 - (P_e / P_1)^m]^3 \tag{17}$$

where $m = 1/n$.

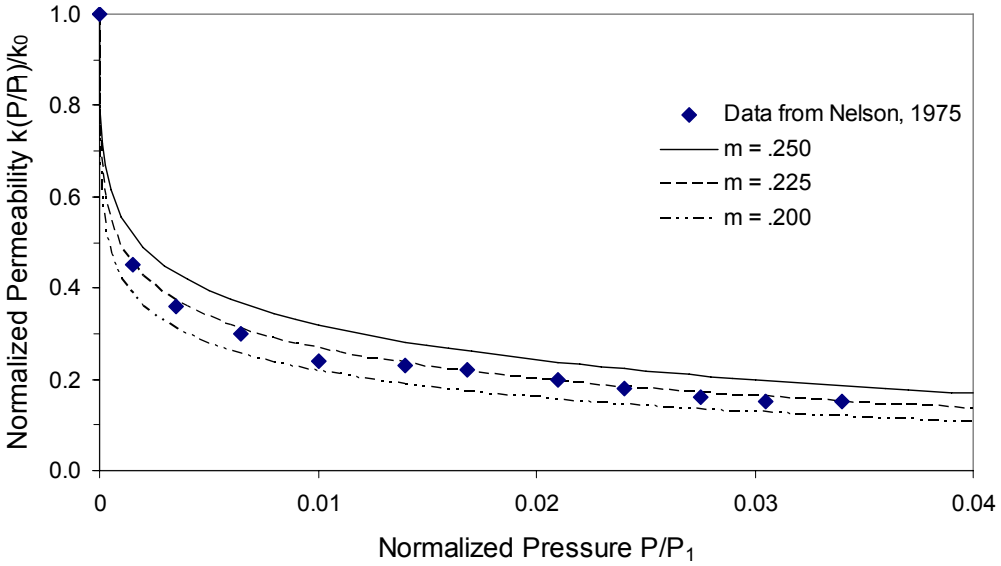

Figure 1. Comparison of Navajo sandstone permeability data with Bed-of-Nails theoretical curves. Data shows excellent correlation, especially when m = 0.225 (*i.e.*, n = 4.44), where m=1/n. Note that there is a data point at $P/P_1=0$ (modified after *Gangi* [1978]).

The permeability measured as a function of confining pressure for cylindrical Navajo-sandstone samples [*Nelson*, 1975] has been fitted using the model given above [*Gangi,* 1975, 1978]. The theoretical curves show excellent agreement with the experimental data (Figure 1). *Kwon et al*. [2001] measured permeability as a function of effective pressure, and their data has also been fitted using the Bed-of-Nails model.

Following the argument in *Gangi* [1975, 1978] and *Carlson and Gangi* [1985], when cracks in rocks are non throughgoing some asperities are in contact when no pressure is applied. To account for such condition, an equivalent "initial pressure" P_i is introduced such that (15) becomes

$$w(P)/w_o = 1-[(P+P_i)/P_1]^m \tag{18}$$

The crack has some initial width $w(0)$ such that

$$w(0)/w_o = 1-(P_i/P_1)^m \tag{19}$$

The linear crack porosity $\phi_L(P)$ is the sum of the crack apertures, $w(P)$ along a line, divided by the length of the line L

$$\phi_L(P) = w(P)/L = \phi_o w(P)/w_o \tag{20}$$

Gangi [1978, 1980, 1981] has shown that the modulus of a crack for the power-law, Bed-of-Nails model is

$$M_{cr} \cong -w\frac{dP}{dw} = \frac{wP_1}{w_o m}\left(\frac{P+P_i}{P_1}\right)^{1-m} \tag{21}$$

In *Carlson and Gangi* [1985] case I, they assume the grain modulus M_g is much larger than the crack modulus M_{cr} such that the modulus of a rock, M_r, is given by

$$1/M_r(P) = \phi_L(P)/M_{cr}(P) + [1-\phi_L(P)]/M_g(P) \tag{22}$$

now becomes (when $M_g >> M_{cr}$)

$$M_r(P) \approx \frac{1}{\phi_L(P)} M_{cr}(P) \tag{23}$$

Using the definition of velocity in a rock

$$V(P) = [M_r(P)/\rho_r(P)]^{1/2} \tag{24}$$

where ρ_r is the density of the rock, and combined with all the previous approximations, the variation of P-wave velocity at "low" effective pressures is given by (for the power-law, Bed-of-Nails model)

$$V(P_e) = V_o[1+(P_e/P_i)]^{(1-m)/2} \tag{25}$$

where P_e and m are defined above, and V_o is velocity at $P_e = 0$. P_i is the equivalent initial pressure, which accounts for the fact that some asperities are in contact at $P_e = 0$.

Elastic wave velocities of thermally cracked rocks measured as a function of pressure [*Ciampa*, 1980] were successfully fitted using this model [*Gangi*, 1981]. *Carlson and Gangi* [1985] fitted the variation with pressure of compressional wave velocities in several rock samples as a function of confining pressure using the same model (Figure 2). A nanofossil chalk data set has also been successfully fitted [*Gangi and Carlson*, 1996] using the power-law Bed-of-Nails model.

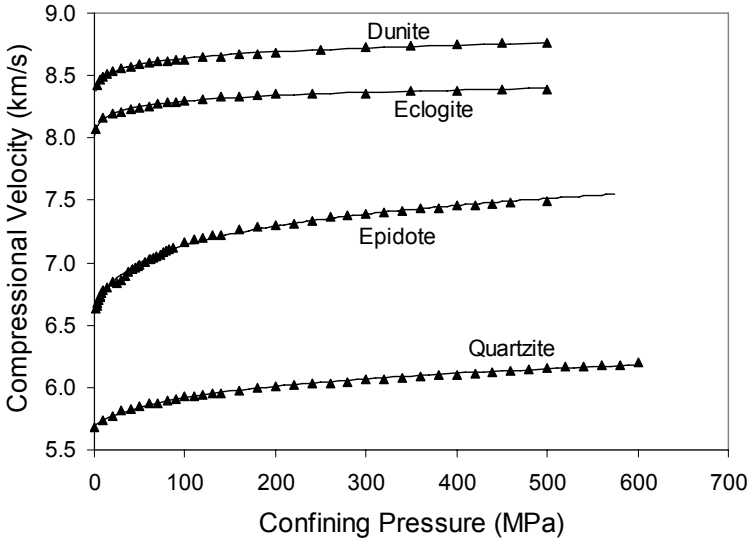

Figure 2. Compressional wave velocity vs. confining pressure (P_p = 0) showing laboratory data (triangles), and Bed-of-Nails fitted curves (equation (25)). Case I model being shown (modified after *Carlson and Gangi* [1985]).

Summarizing, the Bed-of-Nails model has proven to be a very good approximation for the variation with pressure of various mechanical and transport properties, such as velocity and permeability. The Bed-of-Nails model can be used to assess the effect of random errors on the resolution of model parameters from experimental measurements of permeability and P-wave velocity as a function of pressure.

CHAPTER III

METHODS

Estimates of model parameters are usually obtained by fitting experimental data to a given theoretical model. It is important to note the difference between fitting data to a known theoretical model as supposed to fitting the data to an arbitrary function. Some programs can be used to fit data to several functions and choose the one that best fits the data. This seems appealing at first because there is no need to look for a specific equation to begin with; however, the problem is that these equations have no scientific context appropriate for the experimental data being used [*e.g.*, *Motulsky and Ransnas*, 1987]. Even if the equation fits the data well, the results are often meaningless in the context of the experiment. This is why it is important to fit the data to a sound theoretical model known to explain the data being modeled.

Model fitting can be done by linear regression or non-linear regression depending on whether the fitting equation is linear or non-linear in the parameters. When the data allow it, linear models may be used. Linear regression finds values for the slope and intercept that define a straight line (or hyper plane in multi-dimensional space) that best explains a given data set. More precisely, it finds the hyper plane that minimizes the sum of the squares of the vertical distances of the points from the hyper plane. Achieving this goal of minimizing the sum-of-squares is quite simple in linear or multilinear regression, and there is no ambiguity because there is only one minimum for the sum-squared error surface. Non-linear regression is more general, and the goal is to minimize the sum of

the squares (*i.e.*, the misfit) of the distances of the points from the surface [*e.g.*, *Motulsky and Ransnas*, 1987; *Motulsky*, 1996]. It is almost impossible to achieve this directly, as with linear regression and, normally, non-linear regression uses an iterative process to minimize the error.

The process of non-linear regression requires several steps to minimize the error [*e.g.*, *Parrish and Gangi*, 1981; *Motulsky and Ransnas*, 1987; *Motulsky*, 1996]. First, an initial estimate for each of the parameters is input into the program. It is usually possible to plot the data and visually estimate what the values of the parameters are. Once the initial estimates are given to the program, a curve is generated and the sum-of-squares is calculated. The program then adjusts the parameters to make the curve come closer to the data. The most common algorithm to adjust the parameters is the Levenberg-Marquardt algorithm [*Levenberg*, 1944; *Marquardt*, 1963]. The parameters may be adjusted several times until the changes make almost no difference in the sum-of-squares of the distances of the points from the curve, or until there is no significant change in the model parameters on successive iterations. The values of the parameters are reported at the end of the process. The minimized cost function, χ^2 (chi-square) for our study, is also reported by the program as an indicator of the goodness of the fit [*e.g.*, *Bevington*, 1969]

$$\chi^2 = \sum_i \left(\frac{y_i - y(x_i; \mathbf{P}^{(n)})}{\sigma_i} \right)^2 \tag{26}$$

where y_i is the observed i$^{\text{th}}$ value, $y(x_i; \mathbf{P}^{(n)})$ is the calculated value at x_i for the parameter vector $\mathbf{P}^{(n)}$, and σ_i is the uncertainty in the individual values of y_i.

Many physical phenomena, such as the variation of compressional velocity and permeability as a function of pressure, are non-linear in the parameters (*e.g.*, V_o, P_i, and m for velocity). Non-linear fits can be used to estimate the best values of the model parameters and their uncertainties [*e.g.*, *Jennrich and Ralston*, 1979]. Uncertainties in the model parameters are proportional to the overall misfit (also referred to standard error or simply the s.e.) between the model and the data [*e.g.*, *Parrish and Gangi*, 1981], which includes systematic misfit and random experimental error. In the absence of systematic error, the uncertainties in the model parameters depend on the measurement errors (*i.e.*, on the precision of the measurements). If the experimental misfit is large, one or more parameter estimates may be poorly constrained.

In this study, we fit the Bed-of-Nails model to velocity and permeability data sets [*Nelson*, 1975; *Carlson and Gangi*, 1985; *Gangi and Carlson*, 1996; *Kwon et al.*, 2001] to determine the uncertainties of the model parameters, and their sensitivity to the level of error in the data. Other issues such as extrapolation of high-pressure measurements from those made at low pressures, sensitivity of model parameters to measurements made at $P_e = 0$, and effects of using a non-linear fitting routine on the resolution of the model parameters, are also addressed in this study.

The errors in the measured values of an experiment are random and, therefore, it is only one of many possible outcomes (*e.g.*, the actual experiment could be an outlier). By using the determined parameters to generate error-free data sets, and adding Gaussian error to them, we can explore the range of possible outcomes of the experiment. The first step is to fit the Bed-of-Nails asperity-deformation model [*Gangi*, 1975, 1978] to the

experimental data set of interest, and obtain best estimates of the model parameters. These estimates are then used to generate an error-free, "true", or ideal, theoretical model. To model the experiment, we add Gaussian error to the theoretical model and obtain a set of best-fitting parameters. The new fit to this data gives a new set of estimates for the model parameters and their uncertainties. This process yields one realization of the model experiment. Thirty realizations of this procedure are performed to get a statistically meaningful estimate of the range of outcomes of the experiment.

Gaussian errors (*i.e.,* random errors having a Gaussian distribution with mean, $\mu = 0$, and a standard deviation, $\sigma = 1$) were generated using the *Box and Muller* [1958] transformation, given by

$$\xi_1 = \sqrt{-2\ln\eta_1}\cos(2\pi\eta_2) \tag{27}$$

$$\xi_2 = \sqrt{-2\ln\eta_1}\sin(2\pi\eta_2) \tag{28}$$

where η_1 and η_2 are two independent random numbers between zero and one drawn from a uniform distribution, and ξ_1 and ξ_2 are two new independent random numbers, drawn from a Gaussian distribution with $\mu = 0$, and $\sigma = 1$. These random independent numbers are then scaled to generate errors that are introduced in the synthetic data sets.

Because the variations of velocity and permeability with pressure in this study are non-linear, it is pertinent to review some theory on the non-linear least-squares-fitting algorithm and error propagation [*e.g.*, *Bevington*, 1969; *Parrish and Gangi*, 1981; *Bevington and Robinson*, 1992]. Say we have one dependent variable which depends on $\mathbf{x_i}$, the vector of independent variables, $\mathbf{x} = (x_1, x_2, ..., x_m)$, and y_i is the ith value of

dependent variable (Hereafter, bold face type denotes a vector). There are N data points $(y_i, \mathbf{x_i})$, , and.. The objective is to fit the data to a function obtained from a theoretical model (or some fitting function)

$$y = Y(\mathbf{x};\mathbf{P}) \tag{29}$$

where $\mathbf{P}$ is a vector of m parameters, $\mathbf{P} = (P_1, P_2, ..., P_p)$ and $Y(\mathbf{x};\mathbf{P})$ is the expression obtained from the theoretical model.

The problem is to find the best-fitting parameter vector $\mathbf{P}$ by making a least-squares fit of $y = Y(\mathbf{x};\mathbf{P})$ to the data $y_i = y(\mathbf{x_i})$. Following the development of *Parrish and Gangi* [1981] (see also *Bevington* [1969]), we take $y_i = Y(\mathbf{x_i};\mathbf{P})$ and $\mathbf{P} = (P_1, P_2, ...P_p)$, and minimize the sum-squared-error or cost function

$$N\delta^2 = \sum_{i=1}^{N} [y_i - Y(\mathbf{x_i};\mathbf{P})]^2 \tag{30}$$

By solving the set of p simultaneous equations

$$N\frac{\partial}{\partial P_j}\delta^2 \equiv 0 \equiv \frac{\partial}{\partial P_j}\sum_{i=1}^{N}[y_i - Y(\mathbf{x_i};\mathbf{P})]^2 \text{ for } j = 1, m;\ i = 1, N \tag{31}$$

If $Y(\mathbf{x_i};\mathbf{P})$ is a linear function of the parameters, the best fit can be found by simple linear regression. However, if $Y(\mathbf{x_i};\mathbf{P})$ is a non-linear function of one or more parameters (as it is the case of this study), the best fit must be found by other methods. A common approach is to approximate $Y(\mathbf{x};\mathbf{P})$ by the first two terms of its Taylor series expansion to make a linear approximation, and then solve for $\mathbf{P}$ by iteration:

$$-\frac{N}{2}\frac{\partial}{\partial P_j}\delta^2 \equiv 0 \equiv \sum (y_i - Y)\frac{\partial Y}{\partial P_j} \tag{32}$$

Now approximate $Y(\mathbf{x};\mathbf{P})$:

$$Y(\mathbf{x};\mathbf{P}) \cong Y(\mathbf{x};\mathbf{P}^{(0)}) + d\mathbf{P}^{(0)}\ \partial_{\mathbf{P}} Y\Big|_{\mathbf{P}^{(0)}} + d\mathbf{P}^{(1)}\partial_{\mathbf{P}} Y\Big|_{\mathbf{P}^{(1)}} + \ldots \tag{33}$$

where $\mathbf{P}^{(0)}$ is an initial estimate of $\mathbf{P}$ and $Y^{(0)}$ is the estimate of Y computed from $\mathbf{P}^{(0)}$.

We now have

$$\begin{aligned} -\frac{N}{2}\frac{\partial}{\partial P_j}\delta^2 \equiv 0 \equiv \sum \{(y_i - Y_i^{(0)})\ \Big|_{\mathbf{P}^{(0)}} - d\mathbf{P}^{(0)}\partial_{\mathbf{P}} Y\Big|_{\mathbf{P}^{(0)}} - d\mathbf{P}^{(1)}\partial_{\mathbf{P}} Y\Big|_{\mathbf{P}^{(1)}} - \\ \ldots d\mathbf{P}^{(m)}\ \partial_{\mathbf{P}} Y\Big|_{\mathbf{P}^{(m)}}\}\frac{\partial Y}{\partial P_j}\Bigg|_{\mathbf{P}^{(0)}} = \sum \{y_i - Y_i^{(0)} - d\mathbf{P}\partial Y(\mathbf{x};\mathbf{P}^{(0)})\}\frac{\partial Y(\mathbf{x};\mathbf{P}^{(0)})}{\partial P_j} \end{aligned} \tag{34}$$

Letting $\Delta y_i = y_i - Y^{(0)}$ we can write

$$\begin{aligned} \sum \Delta y_i \frac{\partial Y}{\partial P_j}\Bigg|_{\mathbf{P}^{(0)}} &= \sum \{dP_1\frac{\partial Y}{\partial P_1}\Bigg|_{\mathbf{P}^{(0)}} + dP_2\frac{\partial Y}{\partial P_2}\Bigg|_{\mathbf{P}^{(0)}} + \ldots dP_m\frac{\partial Y}{\partial P_m}\Bigg|_{\mathbf{P}^{(0)}}\}\frac{\partial Y}{\partial P_j}\Bigg|_{\mathbf{P}^{(0)}} \\ &= \sum (d\mathbf{P}\partial_{\mathbf{P}} Y)\frac{\partial Y(\mathbf{x};\mathbf{P}^{(0)})}{\partial P_j} \end{aligned} \tag{35}$$

This is a set of simultaneous equations which can be written in matrix form:

$$\begin{bmatrix} \sum \Delta y_i \left.\frac{\partial Y}{\partial P_1}\right|_{\mathbf{P}^{(0)}} \\ \sum \Delta y_i \left.\frac{\partial Y}{\partial P_2}\right|_{\mathbf{P}^{(0)}} \\ . \\ . \\ \sum \Delta y_i \left.\frac{\partial Y}{\partial P_m}\right|_{\mathbf{P}^{(0)}} \end{bmatrix} = \begin{bmatrix} \sum \left(\frac{\partial Y}{\partial P_1}\right)^2 \Big|_{\mathbf{P}^{(0)}} & . & . & \sum \left.\frac{\partial Y}{\partial P_1}\frac{\partial Y}{\partial P_2}\right|_{\mathbf{P}^{(0)}} & \sum \left.\frac{\partial Y}{\partial P_1}\frac{\partial Y}{\partial P_m}\right|_{\mathbf{P}^{(0)}} \\ . & & & & \\ . & & & & \\ . & & & & \\ \sum \left.\frac{\partial Y}{\partial P_1}\frac{\partial Y}{\partial P_m}\right|_{\mathbf{P}^{(0)}} & . & . & . & \sum \left(\frac{\partial Y}{\partial P_m}\right)^2 \Big|_{\mathbf{P}^{(0)}} \end{bmatrix} \begin{bmatrix} dP_1 \\ dP_2 \\ . \\ . \\ . \\ dP_m \end{bmatrix} \tag{36}$$

or

$$\mathbf{Y}^{(0)} = \mathbf{M}^{(0)} d\mathbf{P}^{(0)} \tag{37}$$

therefore

$$d\mathbf{P}^{(0)} = \mathbf{M}^{(0)^{-1}} \mathbf{Y}^{(0)} \tag{38}$$

Now we find the next iteration to $\mathbf{P}$ by setting

$$\mathbf{P}^{(1)} = \mathbf{P}^{(0)} + d\mathbf{P}^{(0)} = \mathbf{P}^{(0)} + \mathbf{M}^{(0)^{-1}} \mathbf{Y}^{(0)} \tag{39}$$

and find $d\mathbf{P}^{(1)}$. The iteration procedure is ended when $\frac{|d\mathbf{P}|}{|\mathbf{P}|}$ is small enough, at which point $\mathbf{P}^{(n)}$ is a vector of best fitting parameters.

$$d\mathbf{P}^{(1)} = \mathbf{M}^{(1)^{-1}} \mathbf{Y}^{(1)} \tag{40}$$

The parameter covariance matrix is given by

$$\mathbf{S_P}^2 = \begin{bmatrix} S_{11}^2 & S_{12}^2 & S_{13}^2 \\ S_{21}^2 & S_{22}^2 & S_{23}^2 \\ S_{31}^2 & S_{32}^2 & S_{33}^2 \end{bmatrix} = S^2 \mathbf{M}^{-1} \tag{41}$$

where the numbers refer to the parameter number (*e.g.*, $S_{11} = S_{P1}$), and the "error" matrix is

$$\mathbf{S_P} = S\sqrt{\mathbf{M}^{-1}} \tag{42}$$

where $\mathbf{S_P}$ is the uncertainty in a given parameter, and S is the misfit (*i.e.,* the standard error of the estimate), which is an estimator of the Gaussian error in the data. The term $\sqrt{\mathbf{M}^{-1}}$ is a constant in the linear case because it depends only on $\mathbf{x_i}$. In the non-linear case, however, $\sqrt{\mathbf{M}^{-1}}$ is not strictly invariant, but depends on different factors such as initial choice of values for model parameters, the level of error, the values of the independent variable(s), and the iteration path, which does not always lead to the same answer. Nevertheless, we expect $\mathbf{S_P}$ to be proportional to S.

To test the hypothesis that

$$\frac{\mathbf{S_P}}{S} = \sqrt{\mathbf{M}^{-1}} \approx const. \tag{43}$$

the variation in compressional velocities with pressure in a quartzite sample reported by *Carlson and Gangi* [1985] was fit to equation (25) with model parameters V_o, P_i, and m, where $m = 1/n$. The data itself shows a typical variation of compressional velocity in rocks as a function of increasing confining pressure; a rapid increase in velocity at low pressures (0-100 MPa), and then slower increase at higher pressures. Using the software Kaleidagraph, the quartzite data were fitted using the Bed-of-Nails asperity-deformation model [*Gangi*, 1975, 1978] yielding approximations for the parameters V_o, P_i, and m (Figure 3). The curve of the theoretical model fits the data quite well, with a standard

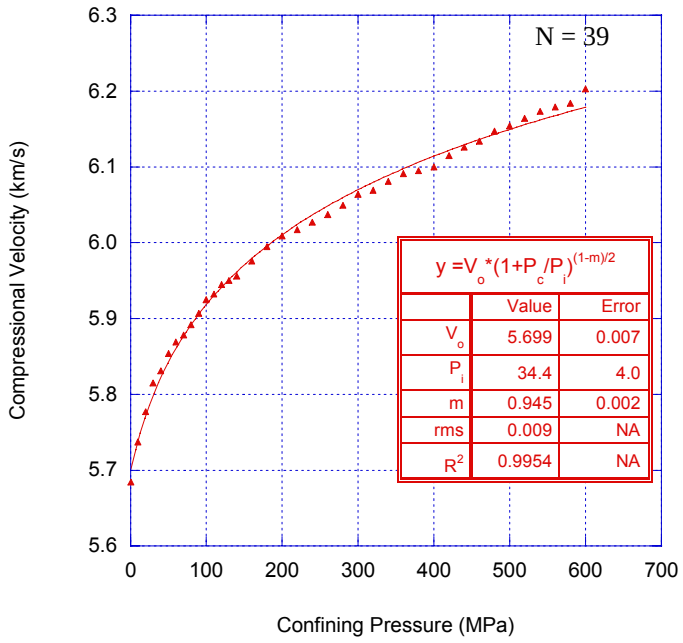

Figure 3. Best fit to quartzite velocity data (triangles) adopting the Bed-of-Nails model. Best estimates for model parameters shown inside the box.

error of just 0.009 km/s, but there is some systematic error detectable throughout the fit. Below 100 MPa, the best-fitting curve tends to underestimate the experimental values, while above 200 MPa the best-fitting curve over-estimates the experimental values, and then underestimates the values above 500 MPa.

The best-fitting model parameters were used to generate an error-free, synthetic data set of compressional-wave velocities as a function of confining pressure adopting the power-law Bed-of-Nails model [*Gangi*, 1975, 1978] given by equation (25). Our procedure is to use the standard error from the initial fit as the standard deviation of the Gaussian error in the model. Figure 4 shows the error-free, synthetic data set as a solid curve bounded by dashed lines, which represent the level of error being introduced, in

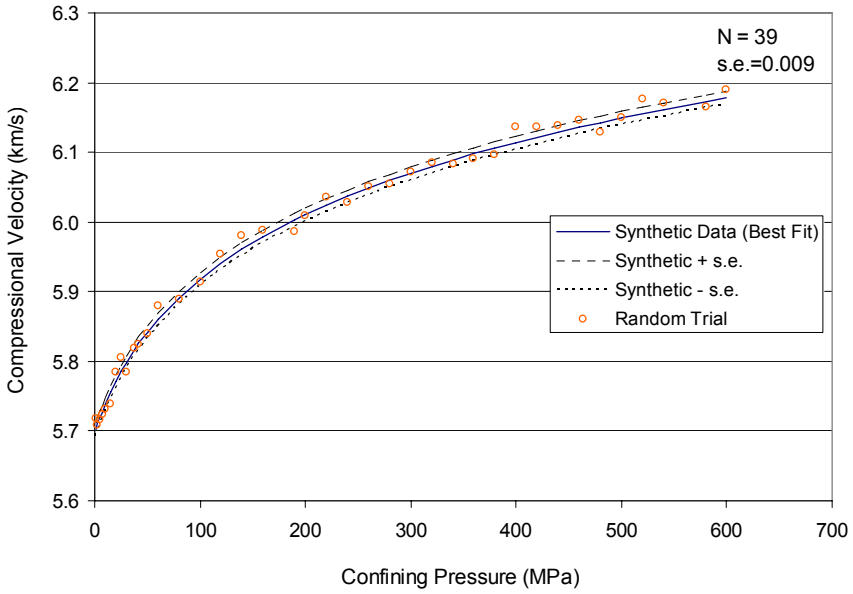

Figure 4. Gaussian Error introduced to error-free, synthetic velocity data set. Best-fitting curve shown as a solid curve, and level of error added is shown by the dashed line. Circles show one of the realizations performed at this error level.

this case the standard error of 0.009 km/s. The open circles show a single realization chosen at random from the total of thirty that were done. Notice that 14 out of 39 data points fall outside the standard error boundaries. This is what we expect when introducing errors drawn from a Gaussian distribution where approximately 32% of the values fall outside one standard deviation from the mean. Note also that there is more scatter in the model than in the real data (Figure 3) because the systematic error in the fit to the experimental data is included in the model random error (Figure 4).

Each of the thirty realizations was fitted using equation (25) and, thus, generated a new set of estimates for the model parameters. To test the hypothesis that the term $\sqrt{\mathbf{M}^{-1}}$ is approximately constant in the non-linear case (equation (43)), we repeated this

Table 1. Summary of numerical results for velocity data showing three different amounts of error introduced.

Error Introduced (km/s x 10^2)*	V_o Uncertainty (km/s x 10^2)*	P_i Uncertainty (MPa x 10^{-1})*	m Uncertainty (x 10^3)*
0.009	0.005	3.5	0.0016
0.023	0.011	8.8	0.0041
0.046	0.024	17.7	0.0082

* Notice the values have been scaled for purposes of showing them together in Figure 5. Uncertainties in parameters are the average value from the 30 realizations.

analysis for two additional levels of random error: 0.023 and 0.046 km/s. The average standard error for each parameter, taken over the thirty trials for each level of error, is given in Table 1, and the results are summarized in Figure 5, which shows the relationship between the parameter uncertainties and the misfit introduced to the error-free, synthetic data sets. In each case, the relationship is clearly linear. Two of the parameters (P_i and m) show a perfect fit with a coefficient of determination of 1. The other parameter (V_o) also shows an excellent fit with a coefficient of determination of 0.9954. The linear relationship between the parameter uncertainties and the misfit indicate that, in fits of this model to experimental data given typical experimental errors, $\sqrt{\mathbf{M}^{-1}}$ is approximately constant, and the parameter uncertainty matrix $\mathbf{S_P}$ is proportional to the misfit S (or simply the standard error). This result is only true in some cases, and in fact we will see this relationship does not hold when working with the permeability data sets (see chapters VI and VII).

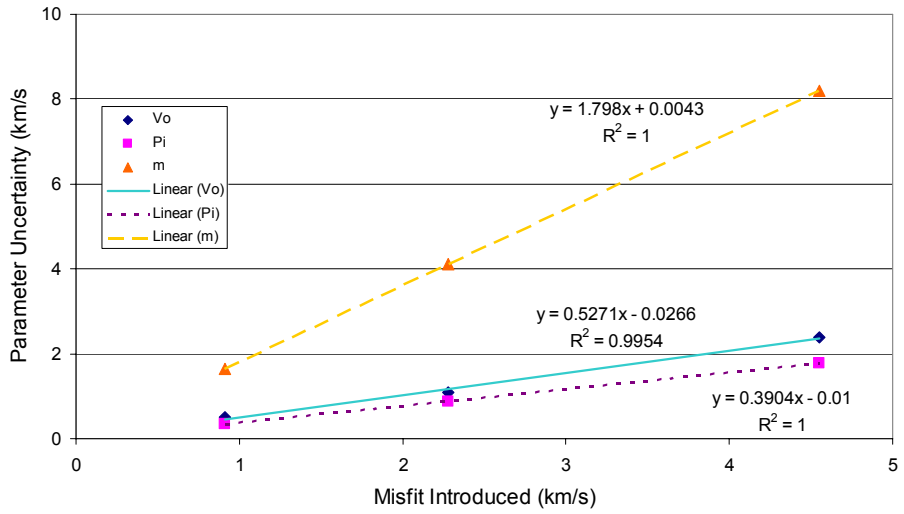

Figure 5. Linear relationship between parameter uncertainty and misfit. Parameters are shown as circles (V_o), squares (P_i), and triangles (m). Linear regressions have been included for each one the parameters, and their corresponding best-fitting equations and correlation coefficients.

CHAPTER IV

EXTRAPOLATION EXPERIMENTS

Extrapolating a fit beyond the range of the data is usually considered bad practice and often avoided. Extrapolation can sometimes be justified if the fit is made to a sound theoretical model [*e.g.*, *LuValle*, 2004]. High-pressure measurements are often difficult and costly to make, which is why trying extrapolation to higher pressures is useful. What we wish to know is how well we can extrapolate experimental data (acquired at pressures between 0 and 100 MPa) to 600 MPa. To answer this question we have used an epidosite data set [*Carlson and Gangi*, 1985] consisting of fifty compressional velocities measured over pressures ranging from 1-500 MPa (See Table A-1).

The complete data set has been fitted (Figure 6) to the Bed-of-Nails asperity-deformation model [*Gangi*, 1975, 1978], yielding best-fitting values for V_o, P_i, and m of 6.62 $\pm$ 0.01 km/s, 12.2 $\pm$ 1.2 MPa, and 0.9323 $\pm$ 0.0014, respectively, with a standard error of 0.017 km/s. The parameter V_o is the zero-pressure velocity, and it is usually very well-constrained by measurements made at low pressures. The parameter m, which ranges from 0 to 1, defines the shape of the curve. It also tends to be well-constrained if enough data are available at low pressures where the largest slope change occurs (in Figure 6 this would be approximately in the range 0-100 MPa). The most variable parameter in the epidosite compressional-velocity data set is P_i, which is the equivalent "initial pressure" (or "stress"). P_i may be poorly constrained because there is no data

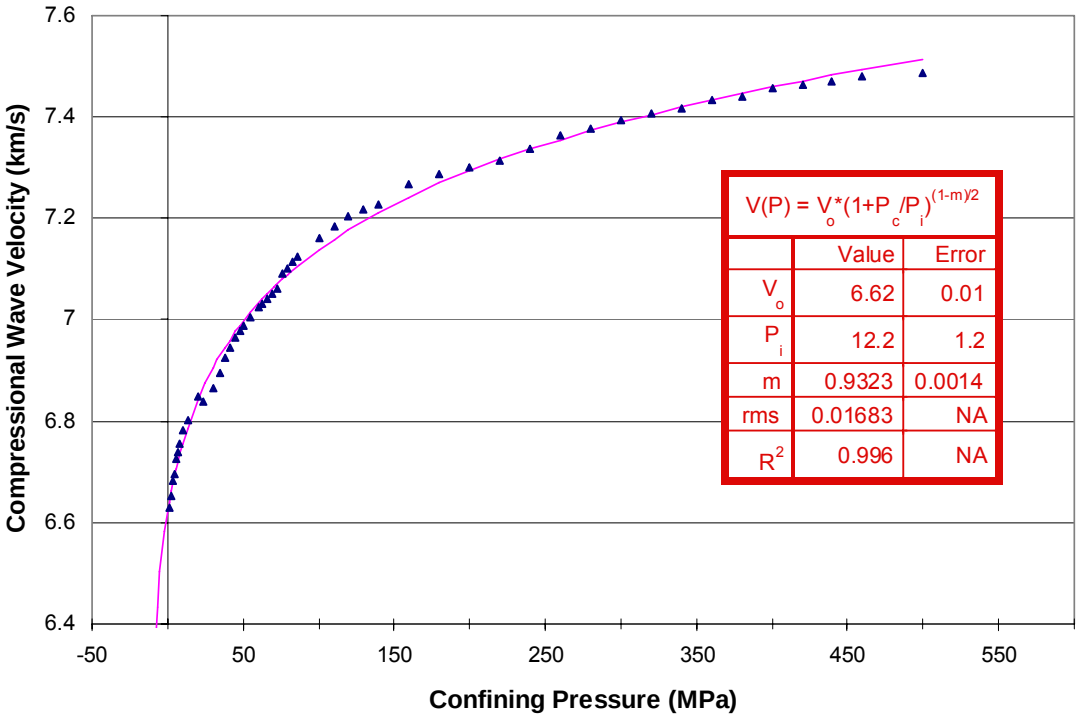

Figure 6. Non-linear fit to epidosite compressional velocity data [*Carlson and Gangi*, 1985]. Values of best-fitting parameters V_o, P_i, m adopting the Bed-of-Nails asperity-deformation model are shown. The experimental data are shown with triangles and best-fitting curve is the solid line.

near this value (*i.e.*, no negative pressure values). Notice the best-fitting curve (Figure 6) has been extended to a theoretical negative pressure to show P_i.

There is some systematic misfit between the model and the data. The best-fitting curve first tends to overestimate the measured values at low pressures of 20-70 MPa, underestimate the measured values at pressures of 70-200 MPa, and overestimate the velocities at high pressures (350-500 MPa). However, the Bed-of-Nails model fits these

data remarkably well and, thus, is a viable theoretical model that explains the variation of velocity with pressure.

To assess the accuracy and precision of velocities at high pressures estimated by extrapolation based on the Bed-of-Nails model, these best-fitting values were used to generate a synthetic, error-free data set, to which we have added random, Gaussian error as described previously. The extrapolation was done by limiting the "experimental" pressures to 0-100 MPa. The idea is to add Gaussian error to the synthetic set, and make a non-linear fit to obtain a best-fitting model. We estimate the velocity at 600 MPa from the error-free model with the added noise. We also varied the number of data points between 0 and 100 MPa (N= 27, 15, 9) to evaluate the extrapolation at different levels of data density. Thirty realizations were done at each one of these levels to assure statistically meaningful results.

The first set of trials was done using 27 data points between 0-100 MPa. The pressures used were the actual pressures. The results are shown in Figure 7 with two data sets plotted; the first is the synthetic data set, and the second is an example chosen at random from the 30 trials to show the extrapolated values above 100 MPa. The values of the parameters V_o, P_i, and m are 6.62 $\pm$ 0.01 km/s, 12.4 $\pm$ 2.1 MPa, and 0.932 $\pm$ 0.004, respectively, where the uncertainties given are the standard deviations, s.d., for each parameter over the 30 trials. The standard error in each one of the parameters over the 30 trials is an estimator of the s.d. of the data. Notice how close the estimates of the parameters are to the true values from Figure 6. The inset in Figure 7 shows the

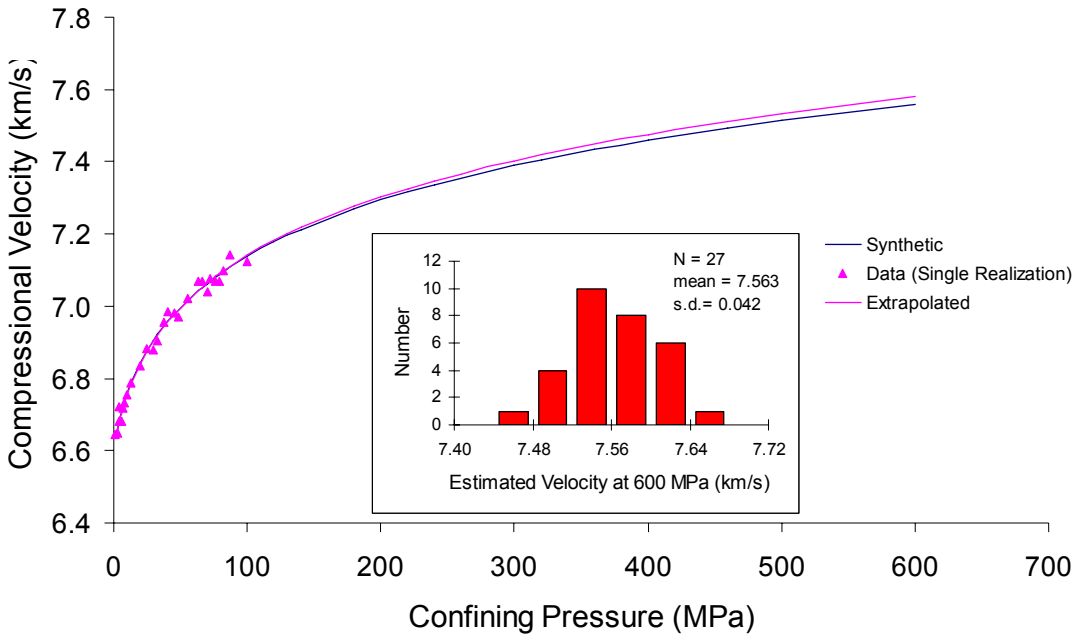

Figure 7. Extrapolated velocities up to 600 MPa using 27 points in 0-100 MPa range. Synthetic data set is shown by solid line, and data from single realization are shown with triangles after 100 MPa. Inset shows distribution of extrapolated values at 600 MPa over 30 realizations. The true value at 600 MPa is 7.560 km/s, and the mean ΔV is 0.003 $\pm$ 0.007 km/s.

distribution of extrapolated values at 600 MPa over the thirty realizations. The mean ΔV (*i.e.*, the mean of the difference between the extrapolated values and the true value, at 600 MPa) is 0.003 $\pm$ 0.007 km/s. Thus, there is no systematic error in the extrapolated velocities. The range of 30 extrapolated velocities is 7.45-7.65 km/s, with a mean and standard deviation of 7.563 km/s, and 0.042 km/s, respectively. The precision of the extrapolated velocities is approximately 0.55%, which compares favorably with the experimental error of 0.22%.

The second set of trials was done under the same conditions as the previous experiment, but this time reducing the number of data points used for the extrapolation

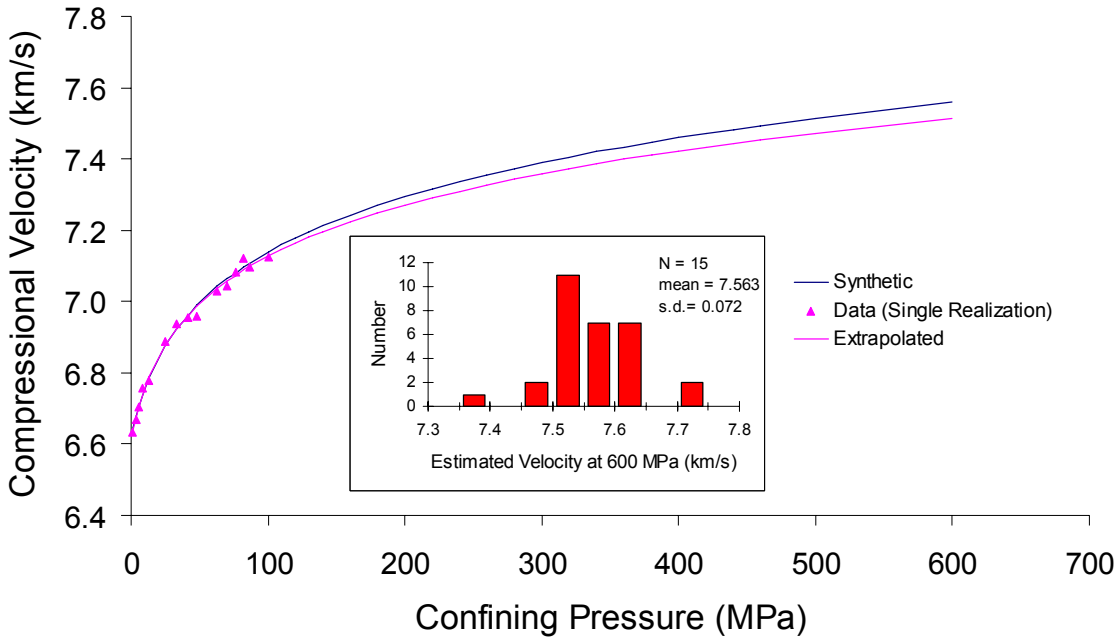

Figure 8. Extrapolated velocities up to 600 MPa using 15 points in 0-100 MPa range. Synthetic data set is shown by solid line, and data from single realization are shown with triangles after 100 MPa. Inset shows distribution of extrapolated values at 600 MPa over 30 realizations (note change of scale). The true value at 600 MPa is 7.560 km/s, and the mean ΔV is 0.003 $\pm$ 0.013 km/s.

from 27 to 15. The results are shown in Figure 8. The values of the parameters V_o, P_i, and m are 6.62 $\pm$ 0.02 km/s, 12.2 $\pm$ 4.2 MPa, and 0.932 $\pm$ 0.008, respectively, where the given uncertainties represent the s.d. for each parameter over the 30 trials. The values of the parameters are still very close to the true values from Figure 6. The uncertainty in P_i has increased significantly compared to the previous case, whereas the uncertainties in V_o and m remain essentially unchanged. The mean ΔV is 0.003 $\pm$ 0.013 km/s. This time, as expected, there is a larger range of extrapolated velocities of 7.35-7.75 km/s, with a mean and standard deviation of 7.563 km/s, and 0.072 km/s, respectively. For N=15, the

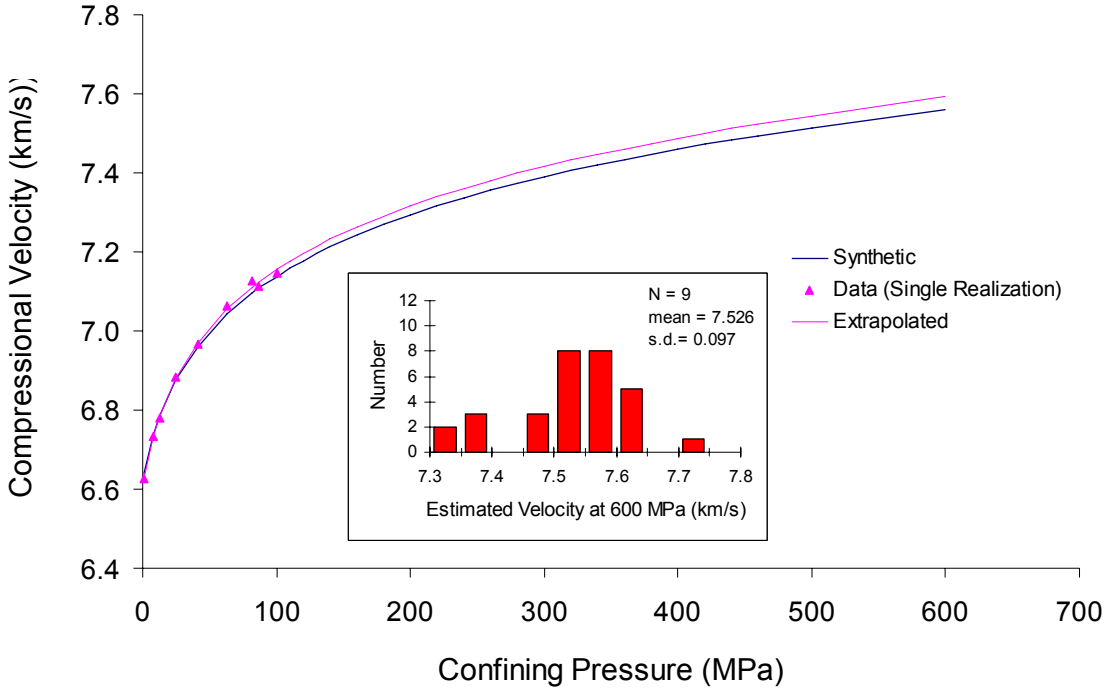

Figure 9. Extrapolated velocities up to 600 MPa using 9 points in 0-100 MPa range. Synthetic data set is shown by solid line, and data from single realization are shown with triangles after 100 MPa. Inset shows distribution of extrapolated values at 600 MPa over 30 realizations (note change of scale). The true value at 600 MPa is 7.560 km/s, and the mean ΔV is 0.034 $\pm$ 0.017.

precision of the extrapolation to 600 MPa is approximately 0.95%, approximately five times larger than the experimental error.

In the third set of trials, we have only used 9 data points in the range 0-100 MPa to make the extrapolation to 600 MPa. The results are summarized in Figure 9. The values of the parameters V_o, P_i, and m are 6.62 $\pm$ 0.02 km/s, 14.0 $\pm$ 5.7 MPa, and 0.933 $\pm$ 0.008, respectively, where the given uncertainties for each parameter represent the s.d. over the 30 trials. The mean ΔV is 0.034 $\pm$ 0.017 km/s, and this time ΔV is very nearly statistically non-zero at the 2σ level. This may be a result of the limited number of data

points used for the extrapolation (*i.e.*, 9) and the values of the parameters reflect this, especially P_i and m. Notice that the value of P_i has increased to 14.0 (from 12.2 and 12.4 in the previous two cases). In this case, the range of extrapolated values has increased to 7.30-7.75 km/s. The mean and standard deviation are 7.526 km/s, and 0.097 km/s, respectively. The precision of the extrapolated velocities is approximately 1.28%.

To better explore the previous case where ΔV is significantly different from the first two cases, a plot of the original best-fitting curve (synthetic, error-free model) and the extrapolated best-fitting curve (average over 30 trails) obtained from only 9 data points has been generated (Figure 10). The misfit between the two curves at 600 MPa is 0.047 km/s. Comparing the model parameters in the two cases, the first one that visually stands

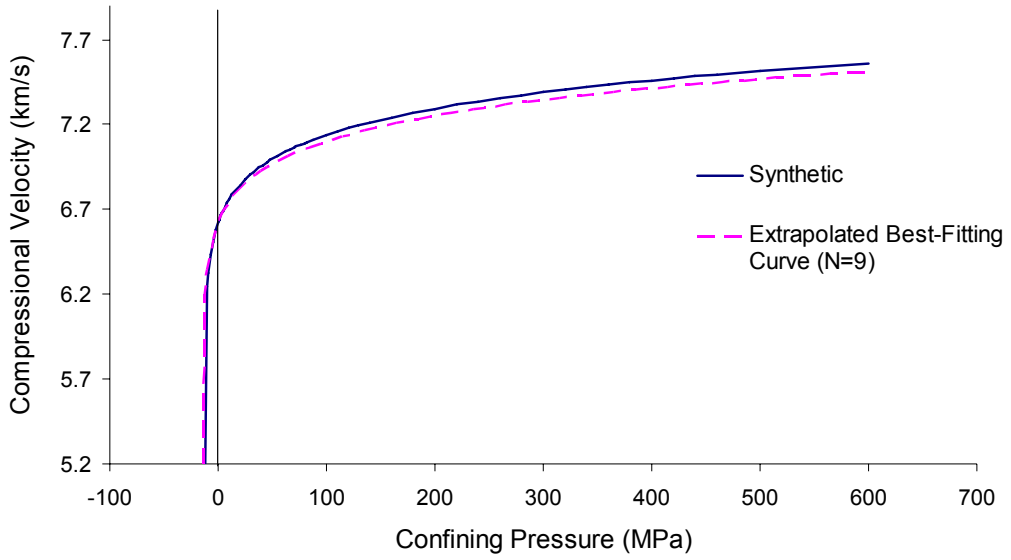

Figure 10. Synthetic (solid line) data set against extrapolated (dashed line) best-fitting curve (obtained from 9 data points in the range 0-100 MPa).

out is m (*i.e.*, the "curvature"). The actual difference is not significant (0.932 in the synthetic data set, and 0.933 $\pm$ 0.008 in the extrapolated data set). The parameter V_o did not change significantly between the two cases and therefore has little effect on the value of ΔV. The other parameter is P_i (12.2 in the synthetic data set, and 14.0 $\pm$ 5.7 in the extrapolated case), and in this case the difference in P_i is ~ 15%. These results suggest that the variation of P_i gives rise to much of the error in the extrapolated value (*e.g.*, where only 9 data points were used), and this inference can be tested by replacing the true P_i value when generating the average extrapolated best figure curve (Figure 11).

The results shown in Figure 11 suggest that the effects seen in the last extrapolation case (Figure 10) are due primarily to the variation in the parameter P_i. The argument for

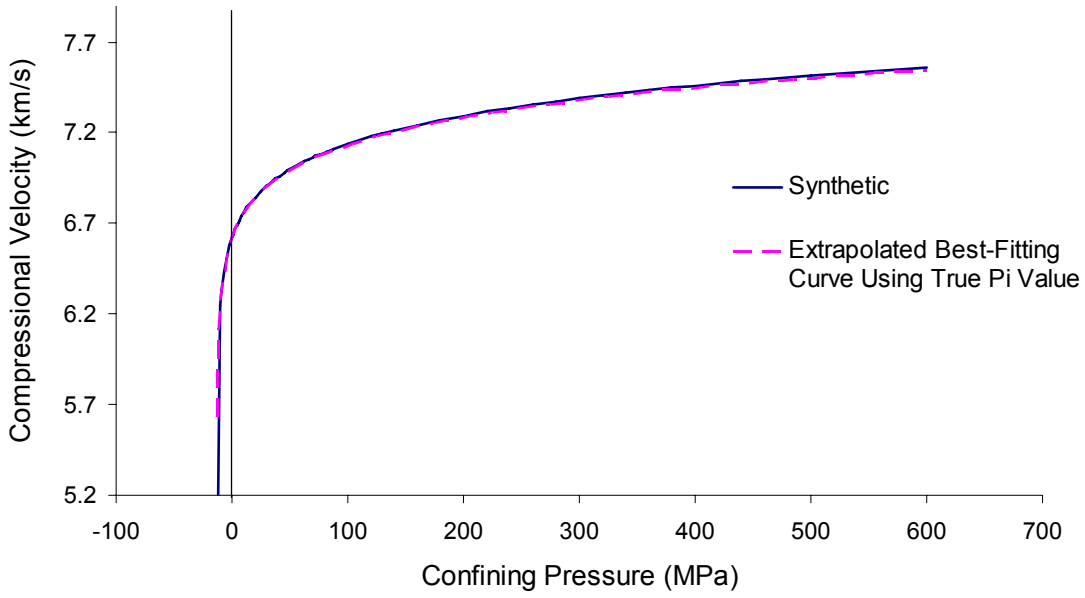

Figure 11. Synthetic (solid line) data set against extrapolated (dashed line) best-fitting curve (obtained from 9 data points in the range 0-100 MPa) using true P_i value (P_i =12.2 MPa). This value has been used to generate an "extrapolated" best fitting curve.

this is that the extrapolated curve generated using the "true P_i" value of 12.2 MPa overlies the synthetic curve. The misfit between the two curves at 600 MPa is 0.013km/s, approximately three times less than the one (0.034 km/s) obtained when the average estimated P_i value (14.0 Mpa) was used (as supposed to using the true P_i).

We have also tested the effects of model error for this data set (Figure 12). In this figure, the experimental data and the best-fitting model are shown in the lower portion of the plot. The upper portion shows the extrapolated velocities at 500 MPa where the highest pressure value used for the extrapolation is the corresponding value at which each data point is shown. For example, the second extrapolated data point from right to left corresponds to 460 MPa. This means that the highest pressure value used to extrapolate this value at 500 MPa was 460 MPa. The next value to the left corresponds to 440 MPa, and this means that the highest pressure value used to extrapolate to 500 MPa was 440 MPa. What the figure shows is that from approximately 240-460 MPa, the systematic error in the extrapolated velocities at 500 MPa increases at a rate of about 3-5 m/s every 20 MPa of pressure. Below 240 MPa, the systematic error in the model increases at a rate of over 10 m/s, and also the error in the extrapolated velocity at 500 MPa increases as we lower the highest pressure value used for the extrapolation. Below 100 MPa, every time we take a data point out for the extrapolation, the error in the value of the extrapolated velocities at 500 MPa increases when compared to the value of 7.510 km/s, as predicted by the best-fitting model. Eventually, it is pointless to keep extrapolating to 500 MPa because the obtained values are far off the expected value.

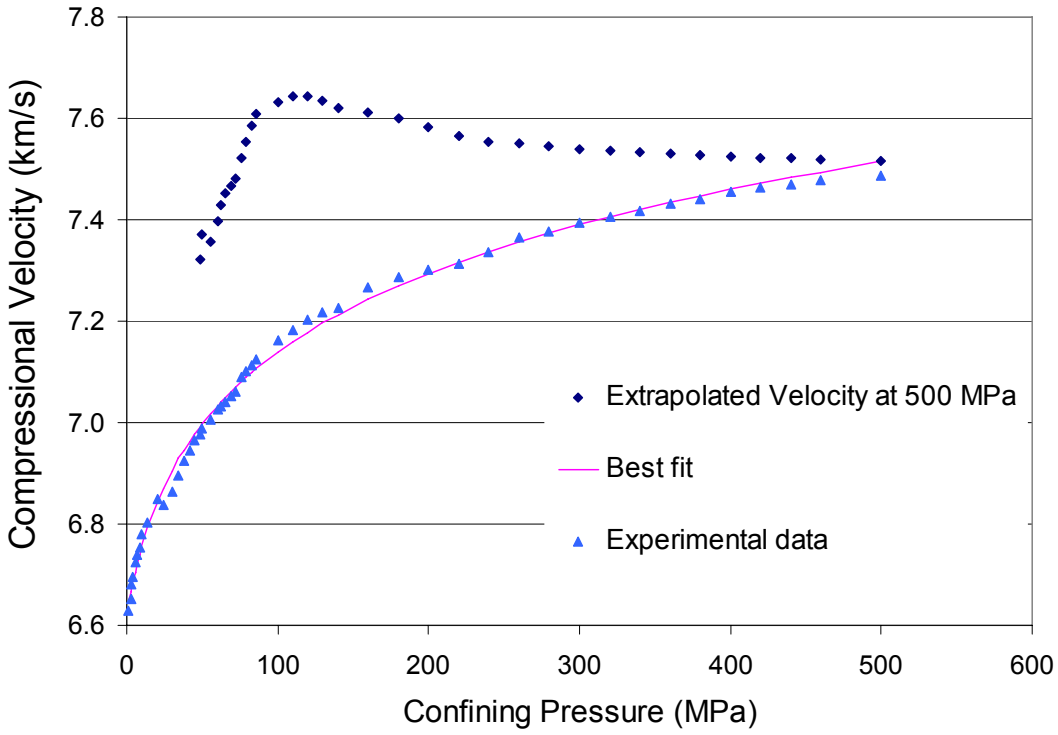

Figure 12. Effects of model error on extrapolated velocities at 500 MPa from epidosite data set. Experimental data (triangles) and best fitting model (solid curve) are shown in lower portion of figure. Upper portion shows extrapolated velocities at 500 MPa where corresponding pressure value was the highest value used to do the extrapolation.

We also tested the effects of adding "truly" zero-mean Gaussian error to this epidosite data set. This arises from the fact that, when adding the Gaussian errors generated by the Box-Muller algorithm (*i.e.,* Gaussian errors with a mean of zero and standard deviation of 1), we are only working with a subset of the numbers generated. This subset may not have (very unlikely) a mean of zero and a standard deviation of one. To test the effects of adding truly, zero-mean error, we have added Gaussian errors to the

synthetic data set generated from the best fit to the original data (Figure 6) as we have done previously. The only difference now is that we have set up two different cases: 1) a subset with non-zero mean error added to the synthetic data set, and 2) a subset with zero-mean error added to the synthetic data set. We have accomplished the second case by subtracting the mean value obtained in the first case from every error value making up the subset of Gaussian errors. After subtracting this value, a new mean is calculated to be zero, but still with the same standard deviation as the previous case.

The results of the two previously mentioned cases are shown in Table 2. The table shows the mean value of the Gaussian error used for each trial (*i.e.*, this is the average value of the errors generated by the Box-Muller algorithm) and its standard deviation. The next column shows the mean, scaled error (*i.e.*, this is the value on the first column multiplied by the original standard error of the data from the best-fit of 0.0168 km/s, so that it can be added to the synthetic velocities), and its standard deviation. The other columns show the best-fitting parameters for each trial. Notice the table has been divided in two cases: 1) the case where non-zero Gaussian error has been added, and 2) the case where zero-mean error has been added. It is also important to note that, the standard deviations for both cases are the same, even though the mean values are not, and this is what we expect.

By looking at the results we can clearly see that there is no difference, statistically, in the values of the best-fitting parameters V_o, P_i, and m obtained for either case. The values of the best-fitting parameters vary from case to case, but are all very close to one another. The standard errors are exactly the same trial in the two different cases.

Table 2. Summary of results for experiment when adding "truly", zero-mean Gaussian error.

Trial	Error (Mean)	s.d.	Scaled Error (Mean)	s.d.	V_o (km/s)	P_i (MPa)	m	s.e. (km/s)
			NON-ZERO GAUSSIAN ERROR ADDED					
Best Fit	-	-	-	-	6.62 ± 0.01	12.2 ± 1.2	0.932 ± 0.001	0.0168
1	0.0462	0.9296	0.0008	0.0156	6.63 ± 0.01	14.1 ± 1.2	0.930 ± 0.001	0.0155
2	0.0771	0.8822	0.0013	0.0148	6.62 ± 0.01	11.3 ± 1.0	0.933 ± 0.001	0.0150
3	-0.1804	1.0114	-0.0030	0.0170	6.62 ± 0.01	13.1 ± 1.2	0.931 ± 0.001	0.0173
			ZERO GAUSSIAN ERROR ADDED					
Best Fit	-	-	-	-	6.62 ± 0.01	12.2 ± 1.2	0.932 ± 0.001	0.0168
1	0.0000	0.9296	0.0000	0.0156	6.63 ± 0.01	14.0 ± 1.2	0.930 ± 0.001	0.0155
2	0.0000	0.8822	0.0000	0.0148	6.62 ± 0.01	11.3 ± 1.0	0.933 ± 0.001	0.0150
3	0.0000	1.0114	0.0000	0.0170	6.63 ± 0.01	13.1 ± 1.2	0.931 ± 0.001	0.0173

* s.d. = standard deviation.
** The column labeled "error" represents the mean value of the errors being added.
*** The column labeled "scaled error" represents the error scaled using the original standard error of 0.0168 km/s to be added to the synthetic velocities.

In summary, we performed three different experiments extrapolating models up to 600 MPa with the only difference being the number of data points used to extrapolate (*e.g.*, 27, 15, 9). We have used a low rms error (0.017 km/s), and this means that the

results of our experiments assume precise measurements of compressional velocity as a function of confining pressure. Also, the theoretical model is known to explain the data over pressures from 0-600 MPa, and this is another very important assumption before attempting to extrapolate. The standard deviation in the range of extrapolated values varied from 0.042 km/s in the case of 27 data points, to 0.097 km/s in the case of 9 data points. These values represent errors ranging from 0.55 to 1.28 %. These results show that we can extrapolate to high pressures (up to 600 MPa) with enough confidence by making measurements at low pressures (0-100 MPa). Even in the case where only 9 data points were used for the extrapolation, the error was still relatively small (1.28%). The results also show that the parameter P_i is the most sensitive to the reduction of data points used for extrapolation, and it dictates to a great extent the scatter present when only using 9 data points. Because of this, it is important to constrain the parameter P_i as well as possible by making measurements at pressures close to zero.

CHAPTER V

VELOCITY AS A FUNCTION OF EFFECTIVE PRESSURE

In the previous section we looked at extrapolation and resolution based on compressional velocities measured over a range of confining pressures only. We expand the analysis to study the resolution of model parameters based on compressional velocities measured over a range of both confining and pore pressures. We have used a marly-nanofossil-chalk data set [*Gangi and Carlson*, 1996] of compressional velocities taken over confining and pore-fluid pressures ranging from 5-60 MPa. The chalk is of Cretaceous age from DSDP Site 357 on the Rio Grande Rise. The wet bulk density of the chalk sample is about 2400 kg/m^3 and the porosity is near 20%. The main objective in this part of the study is to assess the validity of various effective pressure approximations previously given in equations (5-7) using the Bed-of-Nails model [*Gangi*, 1975, 1978].

To illustrate the effects of the different effective-pressure approximations, let us rewrite the Bed-of-Nails model given in equation (25),

$$V(P_{e1}) = V_o \left(\frac{1}{P_i} \right)^{(1-m)/2} \left(P_c + P_i - P_p \right)^{(1-m)/2} \tag{44}$$

$$V(P_{e2}) = V_o \left(\frac{1}{P_i} \right)^{(1-m)/2} \left(P_c + P_i - \chi P_p \right)^{(1-m)/2} \tag{45}$$

$$V(P_{e3}) = V_o \left(\frac{1}{P_i} \right)^{(1-m)/2} \left(P_c + P_i - (\chi_o - aP_d) P_p \right)^{(1-m)/2} \tag{46}$$

Curves of compressional velocity versus confining pressure at constant pore pressure [*Gangi and Carlson*, 1996] are shown in Figure 13. Each of the curves (dashed lines) shown in Figure 13 is a curve of velocity versus confining pressure at constant pore pressure starting at $P_p = 0$ MPa on the left side, and moving to $P_p = 40$ MPa on the right side.

The top diagram shows curves based on the P_{e1} definition (equation (5)), where effective pressure simply equals the differential pressure P_d. In this case, the effective-pressure law, P_{e1}, has the effect of shifting each curve to the right by a distance P_p. The shapes of all curves are exactly the same, and they progressively get shifted to the right by the given pore-pressure increment. The next effective-pressure definition, P_{e2} (equation (6)), though not shown in the figure, has a similar effect of shifting the curves to the right, the difference being that the shift is a fraction of the pore pressure, χP_p, where χ is a constant. The P_{e3} model (equation (7)) is shown at the bottom diagram of Figure 13. In this case the shift in the pore-pressure curves is a function of P_d, $(\chi_o - aP_d)P_p$. Because the shift decreases with increasing confining pressure, curves of velocity versus confining pressure at constant pore pressure converge towards a common value at high values of P_c.

Having illustrated the effects of the various effective-pressure definitions on compressional velocity data, we can now analyze the chalk data [*Gangi and Carlson*, 1996]. A baseline was set for the experiment by fitting only the $V(P_c, 0)$ data (Figure 14) to generate an error budget that can be used for the entire

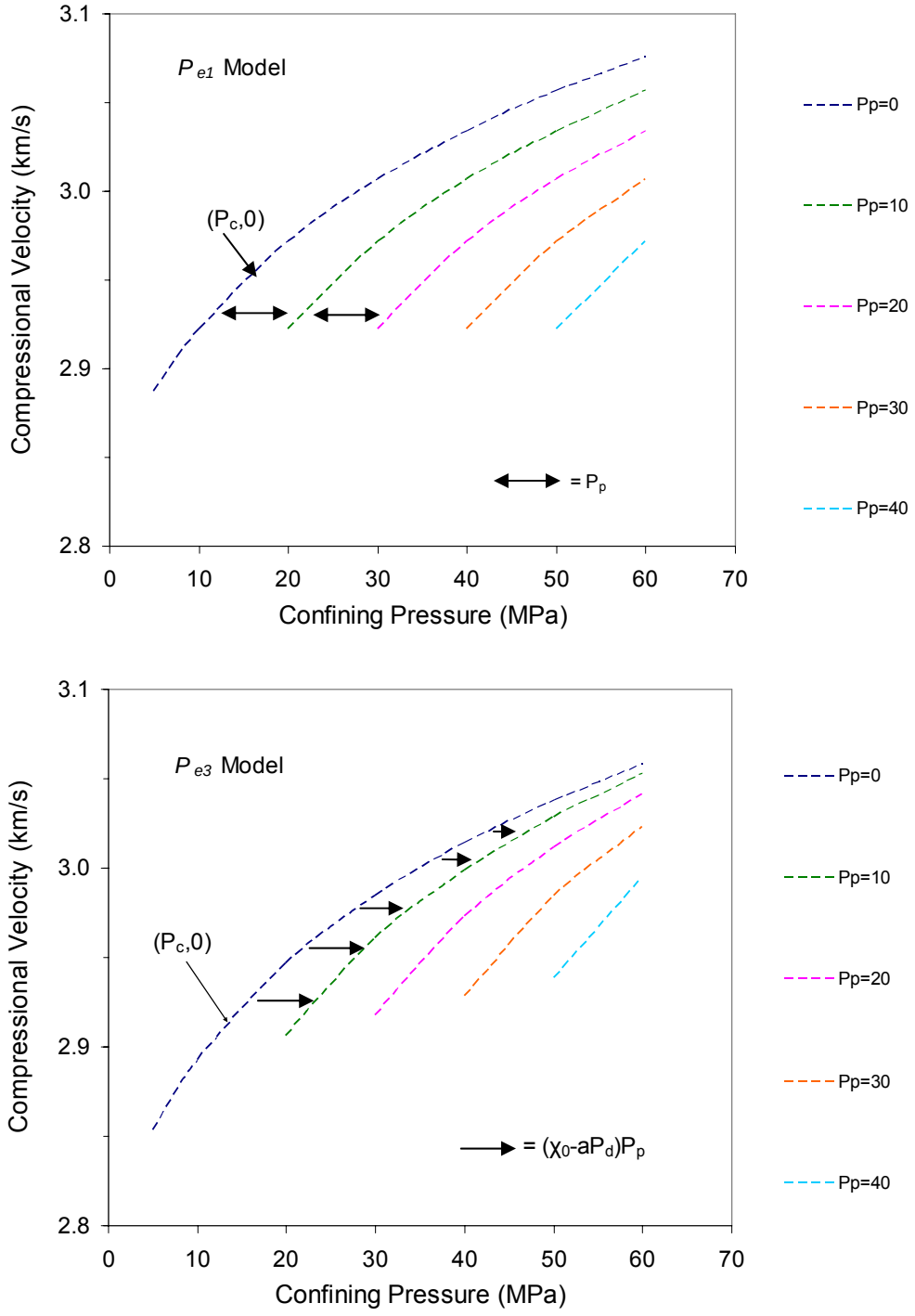

Figure 13. Curves of velocity versus confining pressure at constant pore-fluid pressure showing effects of the various effective-pressure definitions.

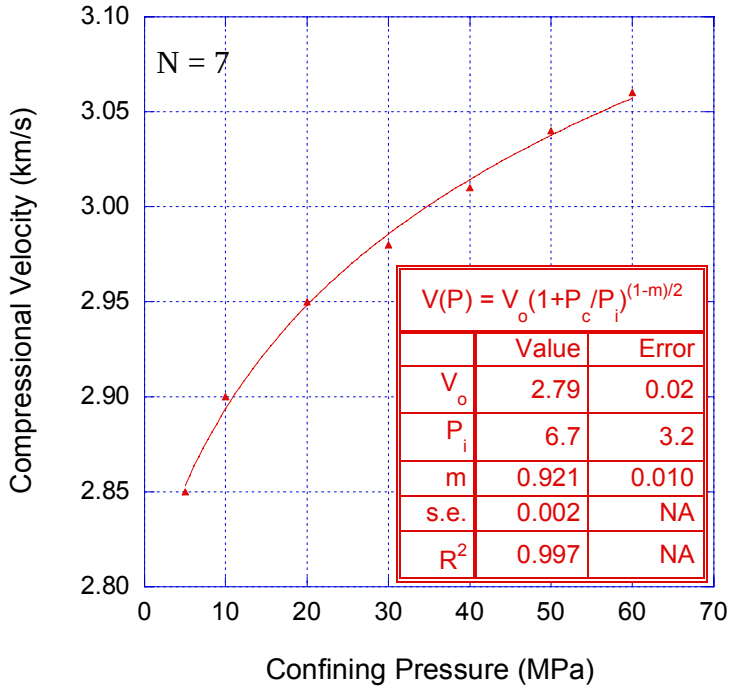

Figure 14. Chalk data fitted with the $(P_c, P_p = 0)$ case. Best-fitting parameters and s.e. shown in inset.

analysis. For $P_p = 0$, the values of the parameters V_o, P_i, and m are 2.79 $\pm$ 0.02 km/s, 6.7 $\pm$ 3.2 MPa, and 0.921 $\pm$ 0.010, respectively, with a standard error of 0.002 km/s, which we take to be the experimental error. We can determine how much systematic error there is when the fit is applied to the entire chalk data set.

The chalk data [*Gangi and Carlson*, 1996] has been fitted using the Bed-of-Nails model [*Gangi*, 1975, 1978] with the three different effective pressure approximations given by equations (44-46), and the results are shown in Figure 15. The constant pore-pressure curves show the same rapid rise of velocity at low pressures, but elevated P_p values have the effect of lowering the velocity. The constant pore-pressure curves tend

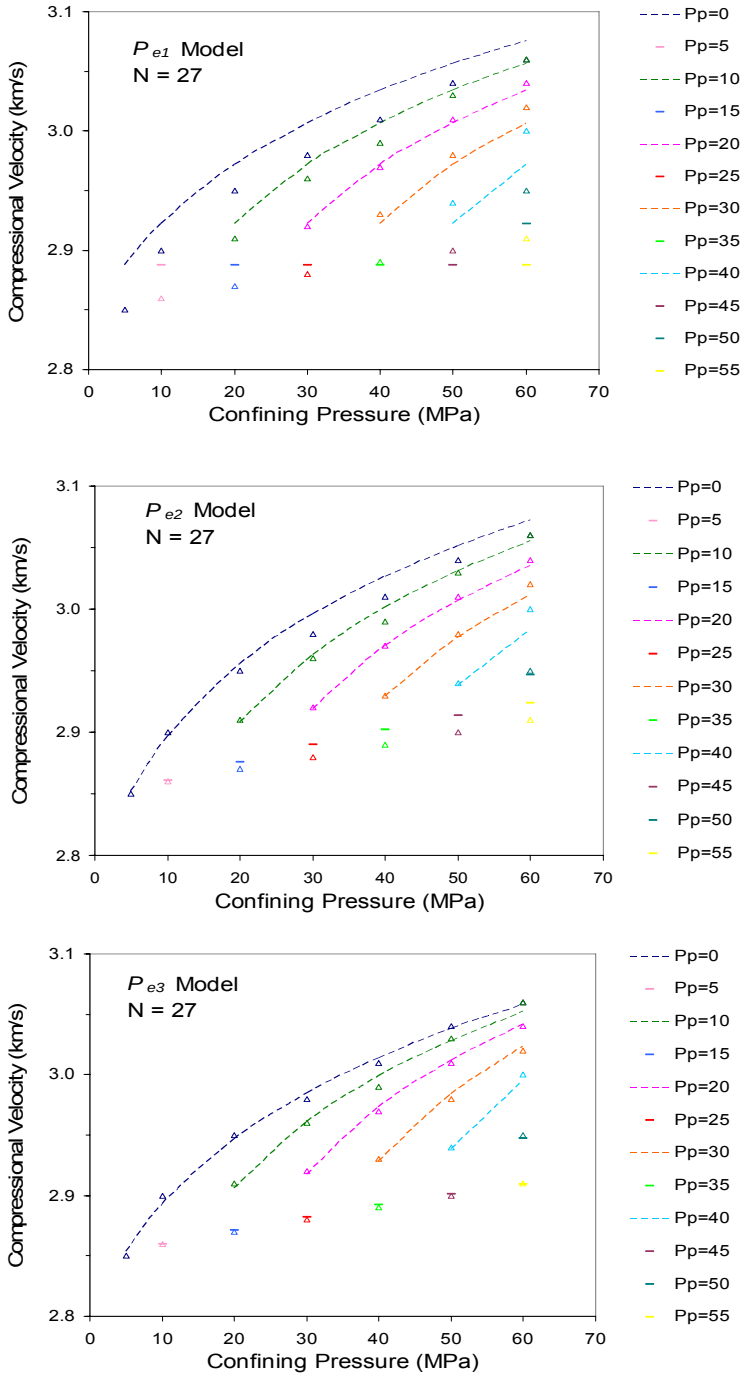

Figure 15. Best-fits to measured compressional velocity in a water-saturated chalk for confining and pore pressures between 0-60 MPa. Experimental data (open triangles) matches color code for calculated constant pore-pressure curves (dashed lines), and calculated single confining/pore-pressure points (dash symbols).

to converge at high P_c values in the P_{e3} case.

In the P_{e1} definition (top diagram in Figure 15), the standard error is 0.019 km/s and is quite large compared to the estimated experimental error of 0.002 km/s. Comparing the P_{e1} definition (top diagram in Figure 15) to the baseline previously set (Figure 14), the excess error is ~0.017 km/s (*e.g.*, the s.e. for the baseline is 0.002 km/s, and the s.e. for the P_{e1} definition is 0.019 km/s). The model overestimates velocities at low P_p and underestimates velocities at high P_p. The excess error is systematic error, and it indicates that the P_{e1} definition used does not explain the data.

Applying the P_{e2} definition (middle diagram in Figure 15) to the data, the standard error is reduced to 0.009 km/s, but there is still excess error compared to the expected measurement error of 0.002 km/s. The systematic misfit decreases as a result of adding the extra parameter χ. There is still disagreement between the experimental data and the corresponding theoretical values, which implies that the P_{e2} definition also does not explain the data.

The P_{e3} definition (bottom diagram in Figure 15) gives the best resolution of all three effective-pressure models with the addition of two new model parameters (*e.g.,* χ_o ,*a*) with respect to P_{e1} . The standard error is ~ 0.004 km/s, twice as large as the expected experimental error of 0.002 km/s, but most of the data is well-explained by using the P_{e3} definition.

A different way to show the same effects of the various effective pressure approximations is to plot the data as a function of effective pressure (Figure 16). This collapses the data to a single trend (at least in the case of P_{e2} and P_{e3}), and the best-

fitting line is now a single line throughout. The same effects as before (Figure 15) of the various P_e models can be seen in this figure. In the P_{e1} model (top diagram in Figure 16), the scatter around the best-fitting curve is an indication that the P_{e1} definition is not valid and more parameters are needed to explain the data. When adding the single parameter χ in the P_{e2} definition, the misfit is significantly reduced but there is still disagreement between the experimental data and the best-fitting line. The last definition, P_{e3}, reduces almost all of the misfit and most experimental data fit the best-fitting curve.

Comparing the uncertainties in the parameters that are common to all the approximations (*e.g.*, V_o, P_i and m), it is easy to see that V_o is well-constrained in all cases with errors of less than 1%. P_i is the most sensitive parameter in all three effective-pressure models, showing a decrease in the error from ~ 84% in the P_{e1} definition to ~23% in the P_{e3} definition. Notice that even for P_{e3} the error in P_i is still comparatively large. The parameter m shows a decrease in error from ~3% in the P_{e1} model to ~0.7% in the P_{e3} model. Overall, the resolution of model parameters V_o, P_i and m gets better going from P_{e1} to P_{e3}, and this is clearly a result of using more information (*e.g.*, more parameters) in the models.

Fitting one real data set represents one realization of a stochastic or random process. Numerical modeling reveals how variable the results might be over a number of experiments. Three synthetic, error-free, data sets have been generated using the estimates of the parameters shown in Figure 16 adopting a particular effective-pressure approximation for each case (*i.e.*, P_{e1}, P_{e2}, P_{e3}). We have introduced Gaussian error to

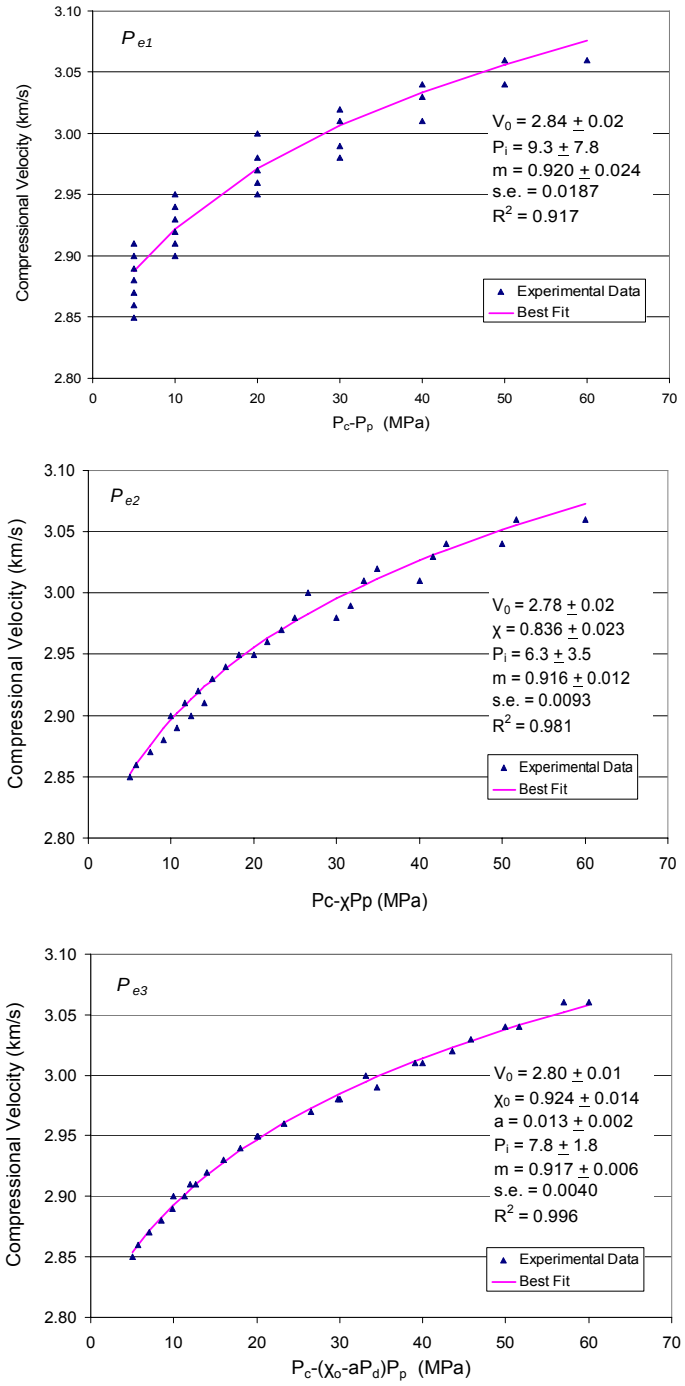

Figure 16. Best-fit to chalk data adopting various effective-pressure models as a function of effective pressure. Notice systematic misfit reduces as the number of parameters in model is increased, and overall resolution increases. N=27 for all three cases.

each data set by the method outlined in the previous section where we use the corresponding s.e. obtained from the original fits. After adding Gaussian error to the three synthetic data sets, a new fit is obtained yielding estimates for the best-fitting parameters. Thirty realizations of this procedure have been done for each effective-pressure approximation to assure statistically-meaningful results. The average parameter values have been estimated from the fits to the synthetic data sets, as well as the s.e. for each one of the effective-pressure approximations.

The results from the numerical experiments are very similar to the ones obtained from the fits to the experimental data (Table 3). Comparing the values of the parameters and their uncertainties to the ones estimated by fitting the experimental data it is clear that the difference is negligible. It is clear from these results that all the values for all parameters from the numerical experiments agree with the values obtained from fitting the experimental data.

It is worth noting the change in the distribution of parameters V_o, P_i and m based on the level of error introduced (Figure 17), since they can be compared for the various effective-pressure approximations. The change in distribution for V_o as the level of error is decreased varies. The first level of error introduced (0.019 km/s) tends to increase the values of V_o (2.80-2.87 km/s), whereas the second level of error (0.009 km/s) tends to lower the values (2.76-2.82 km/s). The lowest level of error introduced (0.004 km/s) tends to confine the range of values to 2.77-2.81 km/s. The widest spread is in P_i as it is the parameter most sensitive to measurement error. The range of P_i is 3-13 MPa for the first two levels of error introduced (*e.g.*, 0.019 and 0.009 km/s). The distribution tightens

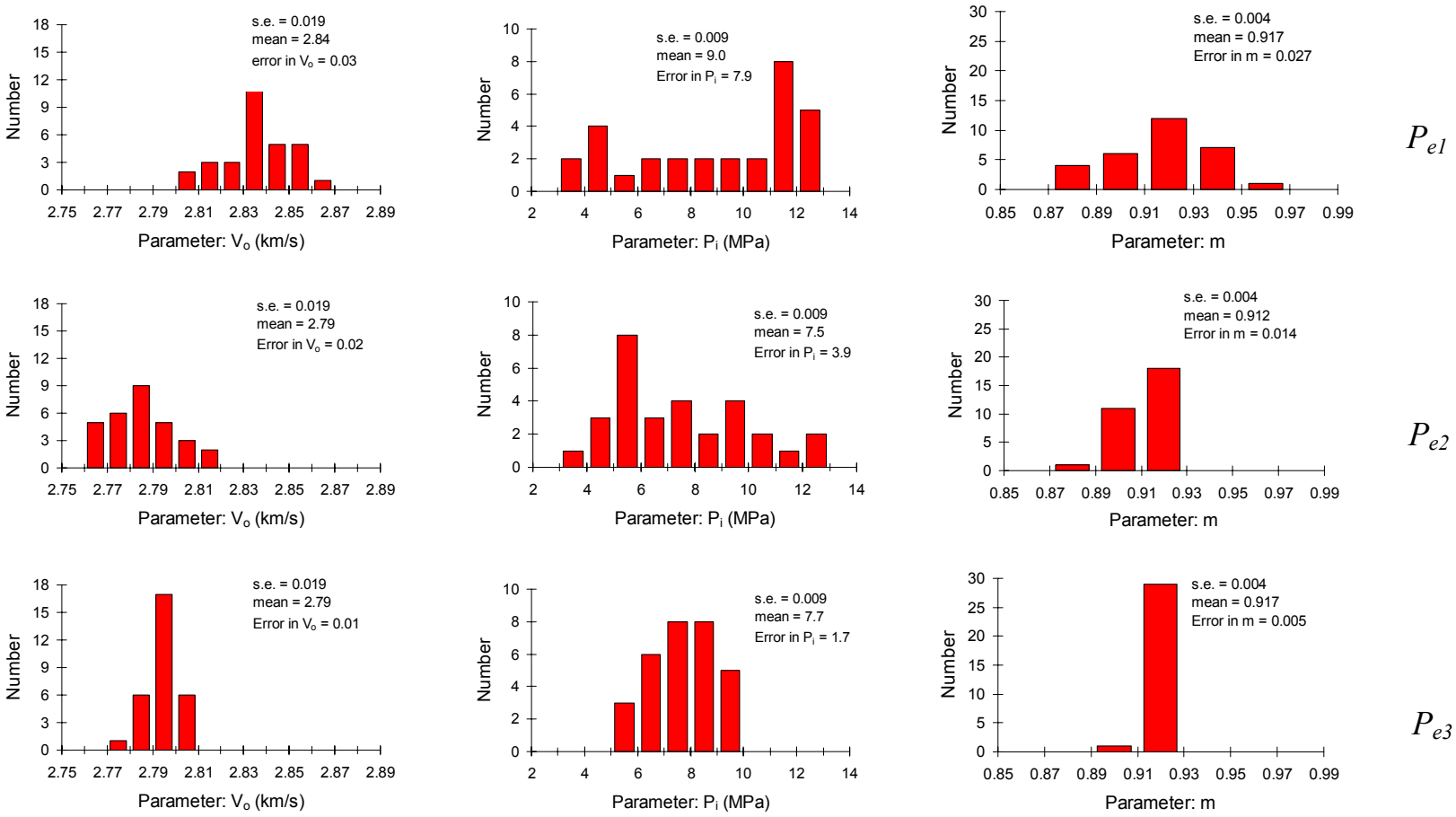

Figure 17. Histograms for best-fitting parameters V_o, P_i and m to synthetic data sets to which Gaussian error has been added. N=27. Each column shows a different parameter. Each row displays the diagrams based on a particular effective-pressure approximation (*e.g.*, going from P_{e1} in the top row to P_{e3} in the bottom row). The given error in the parameters is the standard deviation of the 30 trials, which is an estimator of the error in the parameters.

Table 3. Summary of best-fitting parameters to chalk data and numerical experiments.

P_e * Model	s.e (km/s)	V_o (km/s)	P_i (MPa)	m	χ	χ_o	a (MPa^{-1})
1-E	0.019	2.84 ± 0.02	9.3 ± 7.8	0.920 ± 0.024	-	-	-
1-S	0.019	2.84 ± 0.03	9.0 ± 7.9	0.917 ± 0.027	-	-	-
2-E	0.009	2.78 ± 0.02	6.3 ± 3.5	0.916 ± 0.012	0.84 ± 0.02	-	-
2-S	0.009	2.79 ± 0.02	7.5 ± 3.9	0.912 ± 0.014	0.83 ± 0.02	-	-
2-S	0.019	2.78 ± 0.05	7.1 ± 7.9	0.913 ± 0.028	0.83 ± 0.05	-	-
3-E	0.004	2.80 ± 0.01	7.8 ± 1.8	0.917 ± 0.006	-	0.92 ± 0.01	0.013 ± 0.002
3-S	0.004	2.80 ± 0.01	7.7 ± 1.7	0.917 ± 0.005	-	0.92 ± 0.01	0.013 ± 0.001
3-S	0.009	2.79 ± 0.02	8.6 ± 4.2	0.915 ± 0.013	-	0.92 ± 0.03	0.013 ± 0.003
3-S	0.019	2.78 ± 0.07	6.0 ± 9.1	0.922 + 0.029	-	0.90 ± 0.08	0.010 ± 0.009

* E = Fit made to experimental data.
S = Fit made to synthetic (numerical) data. Values of parameters shown are the average for 30 trials.
Number in P_e column refers to the adopted effective-pressure approximation.

(5-10 MPa) when the smallest error (0.004 km/s) is introduced. In the case of *m*, the behavior is very similar to V_o. The range of values for the first level of error (0.019 km/s) is 0.87-0.97, and the second level of error (0.009 km/s) tends to lower the values to 0.87-0.93. The last level of error introduced (0.004 km/s) once again tightens the distribution of values to 0.89-0.93. The range of values of the parameters V_o, P_i and *m* decrease as the level of error introduced decreases. As we expected, the results agree with fits to the experimental data.

The results from fitting the synthetic data sets using the various effective-pressure approximations also confirm the fact that each subsequent model fits the data better than the previous one, and this is a result of the number of extra parameters that get added for each effective-pressure approximation. The parameters that are unique to a specific effective-pressure approximation (*i.e.*, χ , χ_o , and a) are very important because the resolution of a particular data set depends on the number of parameters used to describe the data. As noted previously, for this particular chalk data set, the P_{e1} approximation lacks enough parameters to explain the data well, which is why it is necessary to expand the model to P_{e2} and add an extra parameter (*e.g.*, χ) to minimize the scatter in the data. P_{e2} is still missing some information, and therefore the fully-expanded P_{e3} definition is necessary to constraint the data set at its best by including two extra parameters, χ_o and a.

To better compare the different effective-pressure approximation results, it is convenient to introduce the same amount of error to two different effective pressure models and see how they behave. Three new sets of numerical experiments were carried out for this purpose. In the first one, the s.e. obtained from fitting the P_{e1} definition to the chalk data (*i.e.*, 0.019 km/s) has been introduced to the synthetic data, but fitted using the P_{e2} definition. In the second and third experiments, the s.e. obtained from fitting the P_{e1} and P_{e2} definitions (*i.e.*, 0.019 and 0.009 km/s) have been introduced to the synthetic data, but fitted using the P_{e3} definition. The results are summarized in Table 3.

In the first experiment adopting the P_{e2} definition, the error (0.019 km/s) appears to be large enough that one of the parameters, in this case P_i, over the 30 realizations,

cannot be resolved from zero (*i.e.*, $P_i = 7.1 \pm 7.9$ MPa). Recall that P_i was the most sensitive parameter to the change of effective-pressure approximations (and therefore change in error introduced), so it is not surprising that having increased the amount of error has resulted in failure to constrain P_i well. All other parameters (e.g., V_o, m, and χ) are still very well constrained with values of 2.78 $\pm$ 0.05 km/s, 0.913 $\pm$ 0.028, and 0.83 $\pm$ 0.05, respectively. Comparing these last three values with the original case where the error was 0.009 km/s, the main difference is that there is an increase in the uncertainty of each one of these parameters by about a factor of 2.

In the second experiment adopting the P_{e3} model, the error introduced (0.009 km/s) has a similar effect on the value of all parameters compared to the previous case. This time though, the parameters V_o, P_i, m, χ_o and a are successfully resolved yielding estimates of 2.79 $\pm$ 0.02 km/s, 8.6 $\pm$ 4.2 MPa, 0.915 $\pm$ 0.013, 0.92 $\pm$ 0.03, and 0.013 $\pm$ 0.003 MPa^{-1}. The error in some of the parameters is high and not ideal for this type of experiment. The two most sensitive parameters in this experiment are P_i and a with associated errors of 49% and 23%, respectively. Notice also that χ_o is distinguishable from one at the 2σ level.

In the last experiment still adopting the P_{e3} model, the error introduced (0.019 km/s) causes P_i to have an associated error of 150%. V_o and m are still well-constrained with values of 2.78 $\pm$ 0.07 km/s, 0.922 $\pm$ 0.029, which represents errors of ~3% in each case. χ_o is still resolvable from one with a value of 0.90 $\pm$ 0.08 (*e.g.*, ~9% error), and a is barely resolvable with a value of 0.010 $\pm$ 0.009 MPa^{-1} (*e.g.*, 90% error).

These results show that the effective-pressure approximation given by P_{e3} is still appropriate to explain the data even at higher than expected levels of error such as 0.009 km/s and 0.019 km/s. Remember that when going from P_{e2} to P_{e3}, two parameters are used (*e.g.*, χ_o ,*a*) in place of χ . These two parameters are still resolvable (even though the uncertainties are high) at higher levels of error. P_i is the parameter that is most sensitive to experimental error in each case. This is an important result because it shows that the effective-pressure relation is well constrained, even when P_i is not well constrained.

After fitting all three effective-pressure models to the chalk data [*Gangi and Carlson*, 1996], and numerically simulating and exploring the implications of these results, it is clear that the P_{e3} definition is the most suitable one for this particular data set, even when the experimental errors are large. One question that arises from the variation of velocity as a function of confining and pore-fluid pressure is how many measurements are needed to constrain the model. We have attempted to address this issue by fitting the P_{e3} definition to only the $P_p = 0$ MPa and $P_p = 10$ MPa experimental data. This experimental subset is made up of 11 measurements. The results are shown in Figure 18.

V_o is very well constrained as it has been in all other experiments, with a value of 2.80 $\pm$ 0.02 km/s (*e.g.*, an uncertainty of less than 0.5%). P_i is very sensitive to the fit and the limited number of measurements used with a value of 10.0 $\pm$ 4.4 MPa, and therefore a large uncertainty of 44%. The parameter *m* is well-constrained with a value of 0.910 $\pm$ 0.013 (*e.g.*, an uncertainty of 1.4%). χ_o has a value of 0.87 $\pm$ 0.17 (*e.g.*, an

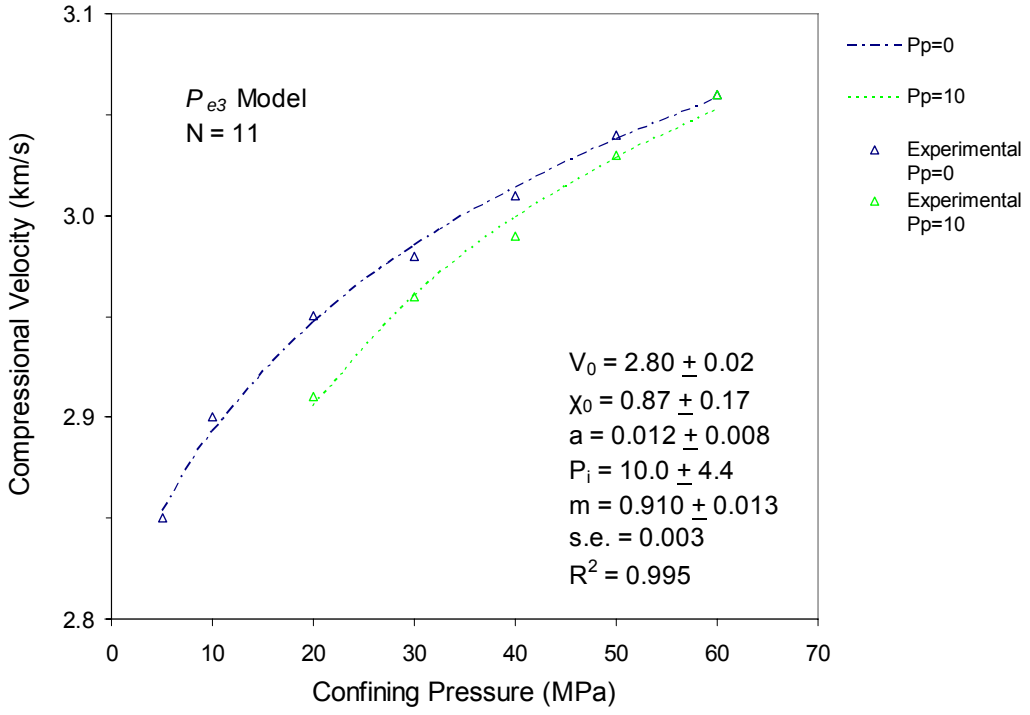

Figure 18. Chalk data fitted using the P_{e3} model for measurements made at $P_p = 0$ MPa and $P_p = 10$ MPa. Best-fitting parameters and s.e. are shown in the Figure.

uncertainty of 20%), and *a* has a value of 0.012 ± 0.008 MPa^{-1} (*e.g.*, an uncertainty of 67%). Clearly, three of the parameters (*e.g.*, P_i, χ_o, and *a*) have large uncertainties. Even that being the case, these results are significant because it is clear that a limited number of measurements can be used to obtain a reasonably well-constrained model.

In summary, various effective-pressure approximations have been successfully modeled by fitting the Bed-of-Nails model [*Gangi*, 1975, 1978] to a nanofossil chalk velocity data set [*Gangi and Carlson*, 1996]. The extent to which the data can be fitted by a particular effective-pressure approximation depends directly on the number of

parameters included in each approximation. The P_{e1} definition, with only three parameters, is not adequate to explain the data sets, and as a result the resolution was poor. By including more parameters in the model (*i.e.*, χ in P_{e2}, and χ_o and a in P_{e3}), the resolution is greatly improved, and the systematic misfit was minimized. Both the original fits to the experimental data and the numerical experiments showed an increase in resolution when progressively higher (*i.e.*, more parameters included) effective-pressure approximations were applied. The resolution of the parameters themselves also reflects this. In the numerical experiments, all the common parameters (*i.e.*, V_o, P_i and m) between the effective-pressure approximations showed an increase in resolution by including more parameters into the model. There was a tendency to tighten the distribution of values in these parameters as progressively higher effective-pressure approximations were used.

Another important point from these experiments is that P_i is the parameter most sensitive to error for this particular data set, and the P_{e3} definition is still appropriate even for the case when the error is high. It is the parameter P_i, and not the effective-pressure model parameters themselves (*e.g.*, χ_o and a) that cause the P_{e3} definition to fail to explain the data when the error is large. Another experiment showed that only using measurements made at $P_p = 0\,\text{MPa}$ and $P_p = 10\,\text{MPa}$, the chalk data [*Gangi and Carlson*, 1996] was successfully fitted adopting the P_{e3} definition, even though the uncertainties in some of the parameters were large. Nevertheless, these results show that only a limited number of measurements are needed to constrain effective pressure models if they are well-chosen and properly made.

CHAPTER VI

PERMEABILITY AS A FUNCTION OF CONFINING PRESSURE

The accuracy of permeability measurements depends upon good experimental set-ups and choice of material can. In this study, we assess the resolution of models based on the Bed-of-Nails model [*Gangi*, 1975, 1978]. Measurements made at low pressures are particularly important in the resolution of model parameters. To study these effects we have chosen a permeability data set consisting of permeability measurements made over a range of confining pressures (0-70 MPa) on a fractured Navajo sandstone sample [*Nelson*, 1975]. Natural fractures in this study were simulated by saw cuts through the sample, as done by *Jones* [1975], and are parallel to the applied pressure gradient.

Nelson [1975] employed a hydrostatic confining pressure vessel with flow-through pore-pressure fluid based on a design developed by *Wilhelmi and Somerton* [1969]. The apparatus measured the flow rate through and the differential pressure of air across the length of the Navajo sandstone sample (cylindrical; 3.5 by 7.5 cm) subjected to conditions of elevated confining pressure and temperature. *Nelson* [1975] fitted his data to an equation based on *Tiller's* [1953] equation

$$k_f = A + BP^{-n} \tag{47}$$

where (k_f) is the fracture permeability, P is the effective pressure, and A, B, and n are positive constants. The same equation was used to describe the pressure variation of the whole-rock permeability (k_r) and the fractured-porous-rock permeability (k_{fr}). These permeabilities are related by

$$k_{fr} = k_r + k_f \tag{48}$$

where the flow in the crack and the pores are parallel so that the total fractured-rock permeability, k_{fr}, is the sum of the porous rock permeability, k_r, and the fracture (crack) permeability, k_f.

Whole-rock permeability was calculated by making measurements of intact rock over a range of confining pressures. Next, samples of the rock taken adjacent to the previous samples containing the artificial fractures are used to calculate the permeability of the fractured porous rock (k_{fr}) (*i.e.*, the total system permeability) using the same range of confining pressures. Fracture permeability (k_f) was calculated by subtracting the whole rock permeability (k_r) from the total system permeability (k_{fr}).

The fracture permeability (k_f) versus pressure from *Nelson* [1975] is shown in Figure 19. The data have been fitted to the Bed-of-Nails model [*Gangi,* 1975, 1978] given by equation (17), where $P_e = P_c$ and $m = 1/n$.

There are a few important points to note in Figure 18. First, the fit itself is very good as indicated by the coefficient of determination $R^2 = 0.998$. The standard error is 0.215×10^{-9} m^2, and the parameters k_0, P_1, and m yield values of $(19.6 \pm 0.2) \times 10^{-9}$ m^2, 2211 ± 360 MPa, and 0.220 ± 0.008, respectively. There is little systematic error. The best-fitting curve goes through all data points, except for the data value at approximately 21 MPa of confining pressure. This data point may be an outlier, and to test this we have re-fitted the experimental data without including this particular point (Figure 20). Comparing the two fits (Figure 19-20), we can see a slight increase in the resolution of

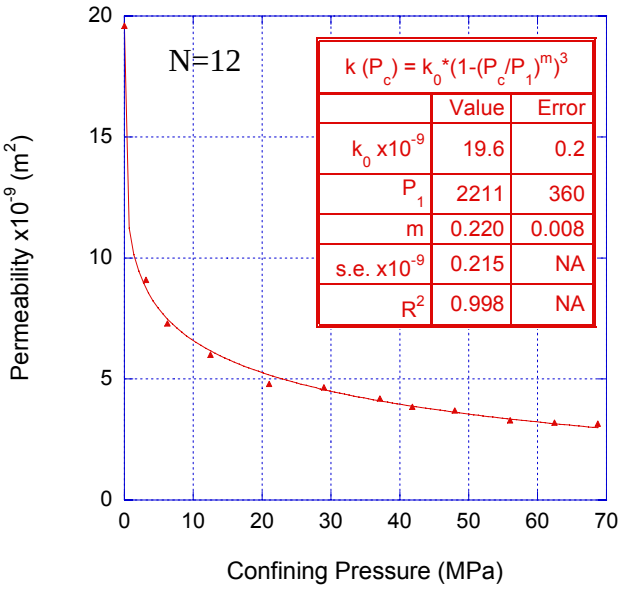

Figure 19. Best-fitting curve to Navajo sandstone permeability data. Best estimates for model parameters k_0, P_1, and m shown. Experimental data (triangles) included a data point at zero pressure.

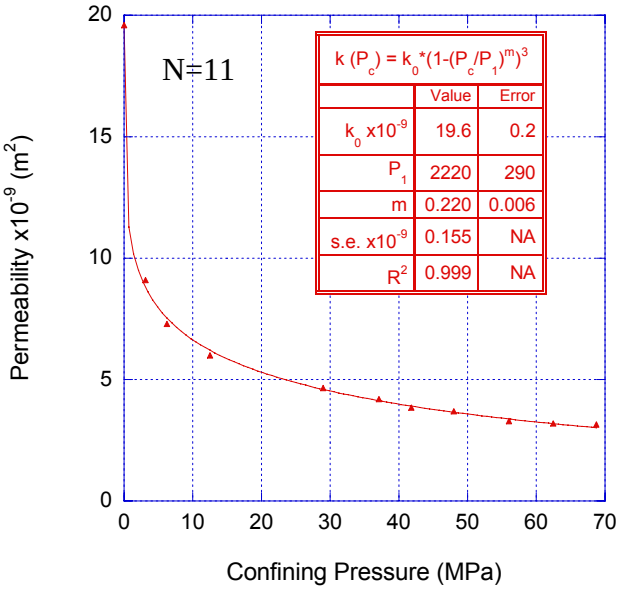

Figure 20. Best-fitting curve to Navajo sandstone permeability data where pressure data point at 21 MPa has been removed.

the model parameters k_0, P_1, and m. The standard error has decreased from 0.215 to 0.155 ($x10^{-9}$ m^2) and this is the most noticeable change compared to the previous fit. This single data point contributes nearly 50% of the overall misfit variance. Even though the change in the value of the parameters (and their associated uncertainties) is not major, the change in the s.e. is significant for the case the data point at 21 MPa has been removed. Based on this finding, the results in Figure 20 were used for the numerical experiments.

The last important point to make from the original fit to *Nelson* [1975] data set (Figure 19) is to note that having data points where the rate of permeability change is high (*e.g.*, near zero pressure) is particularly important. To test the effects of having a

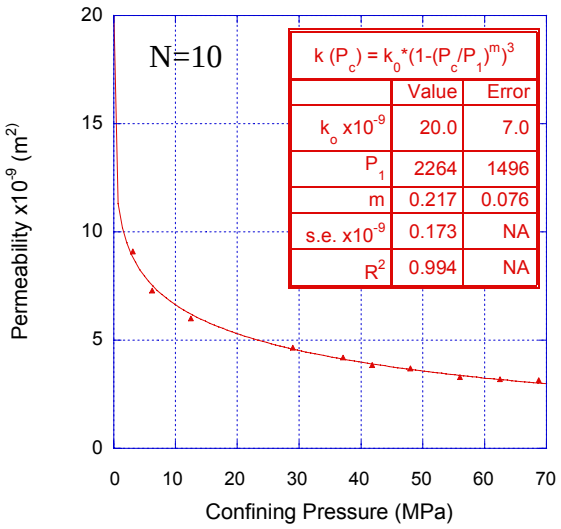

Figure 21. Best-fitting curve to Navajo sandstone permeability data where data point at $P_c = 0$ has been removed. The uncertainties of model parameters k_0, P_1, and m have drastically increased compared to previous fit (Figure 20).

data point at zero pressure, the data has been fitted after removing the experimental data point taken at P_c = 0 (Figure 21). The standard error for the case without the zero-pressure data point has increased from 0.155 to 0.173 (x10^{-9} m^2). There is also evidence of systematic misfit especially at low pressures between 5-13 MPa where the best-fitting curve over-estimates the data points. The results show a major increase (relative to Figure 20) in the uncertainties of all the model parameters, especially on P_1, which has an uncertainty of ~66%. The other two parameters, k_0 and m, both have uncertainties of 35%. Making a measurement at zero pressure (or very close to it) in this type of experiment is extremely important, and has obvious implications in terms of experimental designs and ways to improve such experiments.

These results (Figure 21) suggest that measurements made at low or near zero-pressure affect the resolution (e.g., measured by the uncertainties in the model parameters) of the Bed-of-Nails model parameters. Another question is whether the absence of data at low pressures can be compensated for by having more data. To test these effects, we have performed a series of numerical experiments to address two specific issues. The model parameters in Figure 20 were used to generate three different synthetic data sets; the first case includes a data point at P_c = 0, the second case the data point at P_c = 0 has been removed, and in the third case the data point at P_c = 0 has been removed with the variation that the number of data points has been increased from 11 to 31. The same pressure values as in the experimental data set have been used for the first two cases (except for P_c = 0 in the second case). Gaussian error (the s.e. of 0.155 x10^{-9} m^2 was used) has been added to all three synthetic data sets by the method previously

Table 4. Summary of best-fitting parameters to synthetic data sets based on permeability data as a function of P_c.

Case	Range (MPa)	N	k_o	Avg. Error ($x10^{-9}$ m^2)	s.d.	P_1	Avg. Error MPa)	s.d.	m	Avg. Error	s.d.	s.e. ($x10^{-9}$ m^2)
1	0-70	12	19.6	0.2	0.1	2110	260	130	0.224	0.006	0.004	0.158
2	3-70	11	19.2	5.8	0.9	2080	1220	260	0.227	0.071	0.011	0.174
3	3-70	31	19.2	3.3	0.6	2120	740	140	0.226	0.040	0.007	0.155

* Uncertainties reported for each parameter is the average value over the 30 trials.
** Standard deviations (s.d.) are reported for each parameter over the 30 trials.
*** Standard error (s.e.) for each case is the average value over the 30 trials.

outlined. After adding the Gaussian error, the data were fitted to get new sets of parameters k_0, P_1, and m in each case. Thirty realizations of this procedure were done for each case to assure statistically-meaningful results. The results for the three different cases are summarized in Table 4.

The comparison between the three different cases (Figure 22) is worth noting by looking at histograms of the various model parameters. The true values for each parameter are k_0 = 19.6 $x10^{-9}$ m^2, P_1 = 2220 MPa, and m = 0.221. In the first numerical case where the data point at P_c = 0 was included, the average values of the parameters k_0, P_1, and m were (19.6 $\pm$ 0.2) $x10^{-9}$ m^2, 2110 $\pm$ 260 MPa, and 0.224 $\pm$0.006, respectively, with an s.e. of 0.158 $x10^{-9}$ m^2. The uncertainties in each parameter represent errors of approximately 1%, 12%, and 3%, respectively. The second numerical case where the data point at P_c = 0 was removed, the average values of the parameters k_0, P_1, and m were (19.2 $\pm$ 5.8) $x10^{-9}$ m^2, 2080 $\pm$ 1220 MPa, and 0.227 $\pm$ 0.071, respectively, with an s.e. of 0.174 $x10^{-9}$ m^2. The uncertainties in the parameters are approximately 30%, 58%,

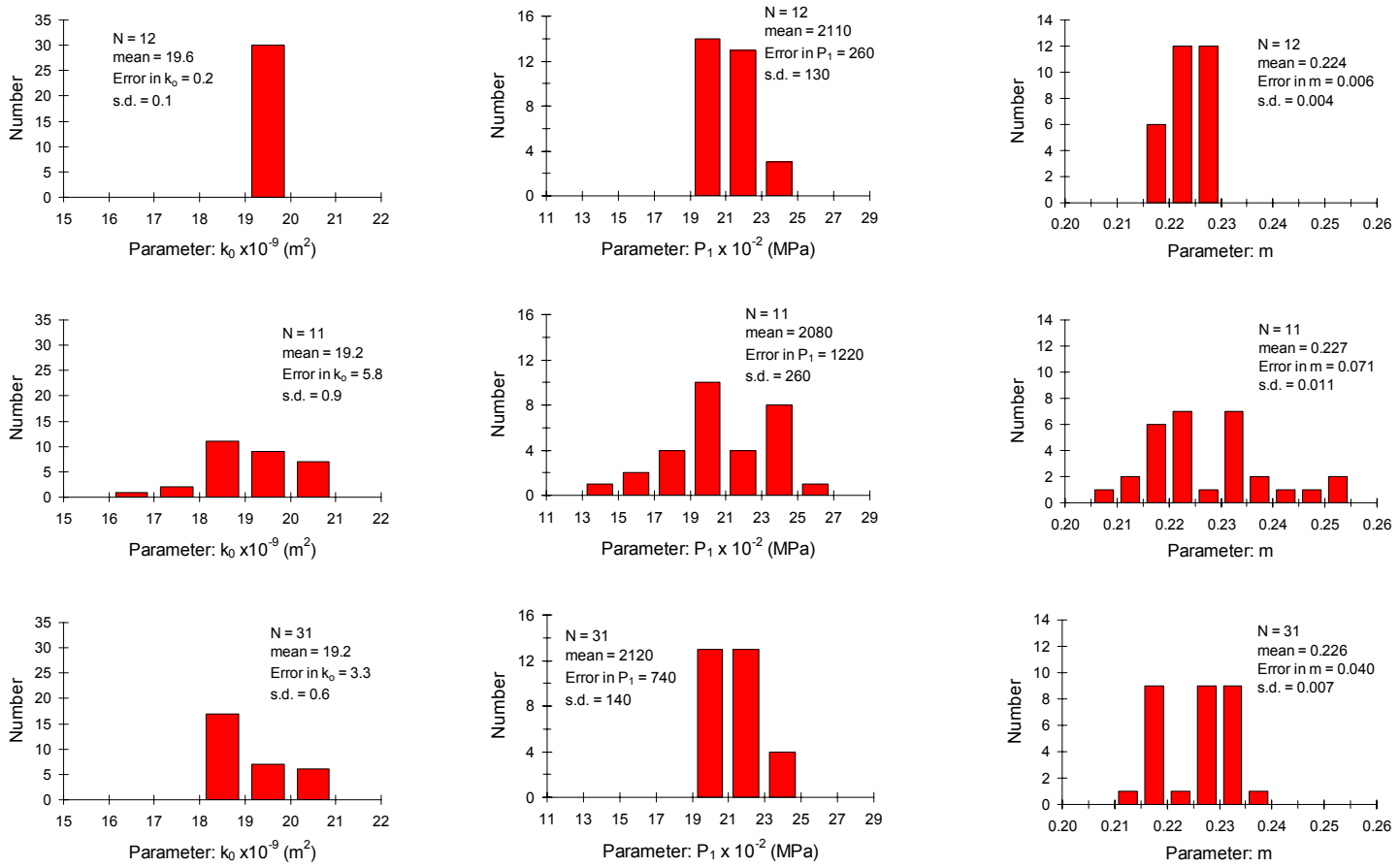

Figure 22. Histograms showing distribution of parameters k_0, P_1, and m for various cases. (a) Zero-pressure data point included in the analysis (0-70 MPa pressure range). (b) Zero-pressure data point removed for the analysis (3-70 MPa pressure range). (c) Higher number (31) of data points included in 3-70 MPa pressure range. Mean and standard deviation are shown for each histogram.

and 31%. In the third case, where the number of data points in the 3-70 MPa pressure range was increased from 11 to 31, the average values of the parameters k_0, P_1, and m are (19.2 $\pm$ 3.3) x10^{-9} m^2, 2120 $\pm$ 740 MPa, and 0.226 $\pm$ 0.040, respectively, with a standard error of 0.155 x10^{-9} m^2, and the uncertainties are approximately 17%, 35%, and 18%. Note that the standard deviations, also given in the table and figure, do not match the average error in the parameters over the 30 realizations. Ideally, the standard deviation should be an estimator of the average error in the parameter, but this condition only holds for the case where the measurement at $P_c = 0$ was included in the analysis. When the data point at $P_c = 0$ is removed, the error space changes and the s.d. is no longer comparable with the average error over the 30 trials. The curvature matrix of the error space is causing these large errors. We will address this issue more closely in the next section.

The uncertainties in all the parameters changed significantly from one case to the other. The parameter P_1 showed the highest sensitivity when the zero-pressure data point was removed (*e.g.*, uncertainty increased from 12% to 58%). Increasing the number of data points to 31 decreased the uncertainty of P_1 by ~24%. The uncertainties in the parameters k_0 and m increased to ~ 30-31% when the zero-pressure data point was removed, and decreased to ~ 17-18% when the number of data points was tripled. The error space changed significantly when the data point at $P_c = 0$ was removed. As a result of this, the increasing (or decreasing) uncertainties in the parameters from one case to another are not proportional to the misfit.

Comparing the true values to each one of the three cases, it is evident that the case with the zero-pressure point included yields better, and closer estimates to the true parameter values. It is also worth noting that the distribution of values for each parameter showed less scatter for the case when the data point at zero pressure was included compared to the other two cases. In the case the zero-pressure data point was included in the analysis, the range of values for k_0, P_1, and m were 19-20 ($x10^{-9}$) m^2, 1900-2500 MPa, and 0.215-0.230, respectively. In the case the zero-pressure data point was removed from the analysis, the distribution of values for k_0, P_1, and m were 16-21 ($x10^{-9}$) m^2, 1300-2700 MPa, and 0.205-0.255, respectively. By increasing the number of measurements to 31, there was a tendency to slightly confine the distribution of values for k_0, P_1, and m to 18-21 ($x10^{-9}$) m^2, 1900-2500 MPa, and 0.210-0.240, respectively, compared to the previous case where the zero-pressure data point was removed, and only 11 measurements were used in the analysis. This is a result of changing the number of degrees of freedom of the fit.

Several conclusions can be drawn from these permeability experiments, but they all converge into a single conclusion, and that is measurements made at very low pressures are particularly important in this type of data. The resolution of all model parameters is significantly better when the data point at zero pressure (or at low pressure) is included. Increasing the number of data points (not including a zero-pressure measurement) can have an important effect of improving the resolution of the model parameters, but the effect is not nearly as large as including a data point at zero pressure. These results

suggest that in order to improve the resolution of such experiments, it is very important to make permeability measurements at low pressures, especially at zero-pressure.

CHAPTER VII

PERMEABILITY AS A FUNCTION OF EFFECTIVE PRESSURE

After looking at permeability as a function of confining pressure only [*Nelson*, 1975], it is useful to extend the analysis to the dependence of permeability not only on confining pressure, but on pore-fluid pressure as well. A Wilcox shale permeability data set [*Kwon et al*., 2001] has been chosen for this purpose. The success of making permeability measurements over a range of confining and pore-fluid pressures, and the ability to constrain theoretical models, depends on many factors such as material of choice, pressures at which measurements are made, and sample-to-sample variation. In this part of the study, the main objective is to assess the resolution of parameters based on the Bed-of-Nails model [*Gangi*, 1975, 1978] given by equation (17) and the implications for the design of permeability experiments.

Kwon et al. [2001] measured the permeability of Wilcox shale parallel to bedding by the transient pulse technique [*Brace et al*., 1968; *Sutherland and Cave*, 1980; *Trimmer*, 1981]. *Kwon et al*. [2001] chose this bedding orientation because the permeability is higher than when the orientation is perpendicular to bedding, and there are wider permeability variations over the range of conditions imposed.

The samples used by *Kwon et al*. [2001] were prepared from shale core of the Wilcox formation in West Baton Rouge Parish, Louisiana recovered from a depth of ~3955 m. The clay content of the core ranged from 40 to 65%. Four different samples were used in the experiment; three of them were taken from the same stratigraphic

horizon of a core, and the remaining one had a similar lithology (taken from core only 0.2 m deeper than the first one). The individual cylindrical samples prepared from the core were 25.4 mm long and 12.5 mm in diameter. Samples were immersed in a 1 *M* solution of NaCl (density of 1040 kg/m^3 [*Wolf et al*., 1979]) for more than 2 days to introduce as much fluid into the pores as possible. Once the pore fluid was introduced, the confining and pore-fluid pressures were increased stepwise to the desired experimental conditions, making sure the values did not exceed the ultimate value of $(P_c - P_p)$ at which permeability was to be measured. Experimental conditions $(P_c - P_p)$ ranged from 3 to 12 MPa, with confining and pore-fluid pressures ranging from 13 to 45 MPa, and from 10 to 42 MPa, respectively. A total of 33 permeability measurements were made with a reported uncertainty of $\pm$ 10%.

To measure permeability, a step change ($\leq$ 15% of initial pore-fluid pressure, P_p) in the fluid pressure was imposed at one end of a cylindrical sample. The pressure difference across the sample then decreases with time

$$(P_{up} - P_{dn}) = \Delta P_i e^{-\alpha t} \tag{49}$$

or

$$\ln(P_{up} - P_{dn}) = \ln(\Delta P_i) - \alpha t \tag{50}$$

where P_{up} and P_{dn} are the upstream and downstream pressures, respectively, at the ends of the sample, ΔP_i is the pressure step change at one end of the sample imposed at t = 0, and α is given by

$$\alpha = (kA/\eta\beta L)(1/V_{up} + 1/V_{dn}) \tag{51}$$

where k is the permeability, A and L are the cross-sectional area and length of the sample, respectively, η is absolute (dynamic) viscosity of the fluid, β is compressibility of the fluid, and V_{up} and V_{dn} are the upstream and downstream reservoir volumes, respectively. α can be found by linear regression (equation (50)). Permeability can be calculated from (51).

The permeability measurements from all four samples were used to determine an effective-pressure law for fluid flow using both the ratio-of-slope method [*Walls and Nur*, 1979; *Bernabe*, 1986, 1987] and the cross-plotting method [*Walsh*, 1981; *David and Darot*, 1989]. The variation of permeability with effective pressure from *Kwon et al*. [2001] was modeled by linearizing the Bed-of-Nails model [*Gangi*, 1975, 1978] in (17),

$$\log[1-(k/k_o)^{1/3}] = m\log P_e - m\log P_1 \qquad (52)$$

where the slope is m and the intercept is $-m\log P_1$. Notice that the parameter k_o is included as part of the dependent variable in this linear approximation. To estimate the model parameters, *Kwon et al*. [2001] did a grid search [*e.g*., *Bevington*, 1969] to find k_o, with linear regression to find P_1 and m (Figure 23). The parameter m is the slope of the best-fitting line, and P_1 was calculated from $-m\log P_1$.

The best-fitting parameters k_0, P_1, and m were determined for the effective-pressure approximation $P_{e1} = P_d$ given by (5). *Kwon et al*. [2001] obtained best-fitting values for k_0, P_1, and m of $1\text{x}10^{-17}$ m^2, 19.3 $\pm$ 1.6 MPa, and 0.159 $\pm$ 0.007, respectively, the last two from the regression shown in Figure 23. The s.e. of the fit, not reported by *Kwon et al*. [2001], was calculated in this study to be $1.20\text{x}10^{-20}$ m^2.

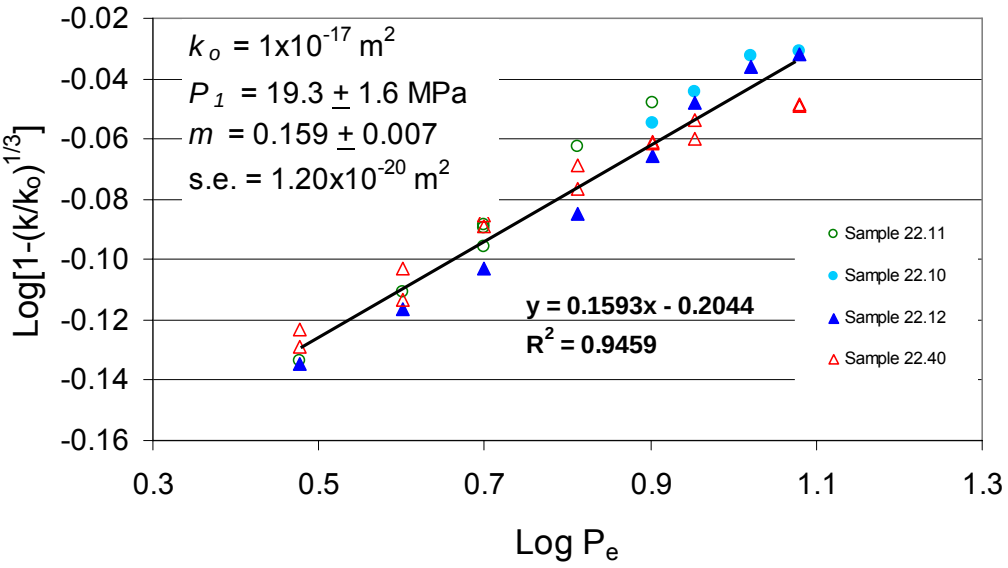

Figure 23. Permeability-effective pressure relationship for Wilcox shale samples. The slope of the line is equal to m, and the intercept is equal to $-m \log P_1$. The experimental data (diamonds) comes from four different samples used by *Kwon et al*. [2001] (modified after *Kwon et al*. [2001]).

In our study, we model the permeability data in *Kwon et al*. [2001] using a non-linear method. The reason for doing this is to compare our results when using a non-linear fit to the linearized approach used by *Kwon et al*. [2001], and explore the differences in the error spaces for each case. When the experimental data behaves in a non-linear fashion, as it is the variation of permeability with effective pressure, it is preferable to model the data using a non-linear fit [*Motulsky*, 1996].

The Wilcox shale permeability data set [*Kwon et al*., 2001] has been fitted (Figure 24) using a non-linear fitting routine using the effective-pressure approximation P_e equals the differential pressure P_d, which itself is the difference between the confining pressure P_c and the pore-fluid pressure P_p. There is no evidence of systematic misfit,

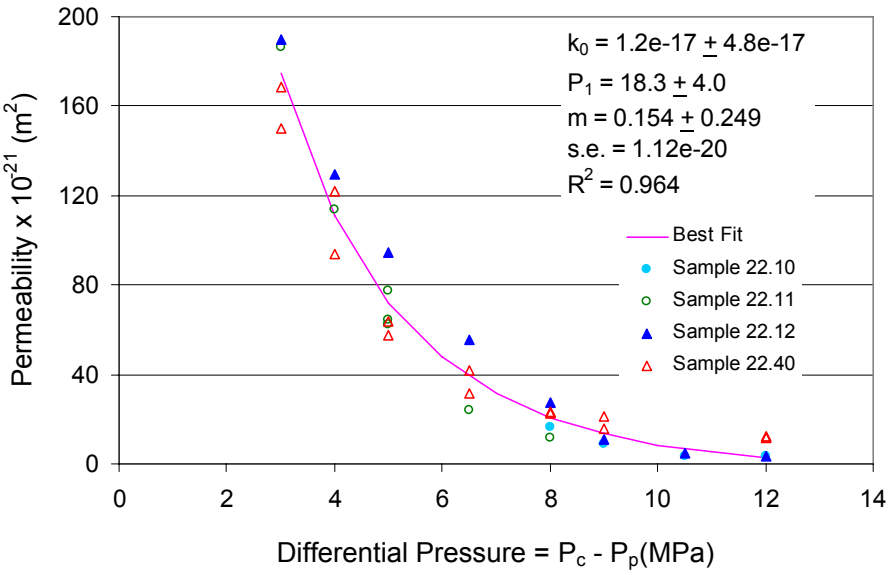

Figure 24. Best-fitting curve (solid line) to permeability experimental data using a non-linear fitting method. Four different samples are shown in the figure. Notice values for best-fitting parameters on the right side.

which suggests that no additional information (*e.g.*, additional parameters) can be obtained from the data. The study by *Kwon et al*. [2001] shows no evidence that the fit could be improved by using other effective-pressure approximations including more parameters such as $P_e = P_c - \chi P_p$ because χ was statistically indistinguishable from 1. The lack of systematic misfit justifies why the P_{e2} model cannot be successfully resolved. Because of this, only the effective-pressure approximation $P_{e1} = P_c - P_p = P_d$ (equation (5)) will be considered for the numerical experiments.

All three parameters were directly estimated from the fit yielding values of k_0, P_1, and m of $1.2\text{x}10^{-17} \pm 4.8\text{x}10^{-17}$ m^2, 18.3 $\pm$ 4.0 MPa, and 0.154 $\pm$ 0.249, respectively, with

an s.e. of 1.12×10^{-20} m^2. The s.e. is reasonable compared to the one calculated previously (*e.g.*, 1.15×10^{-20} m^2). Clearly, the resolution of all model parameters is very poor, especially k_0 where the uncertainty is approximately 400%. This uncertainty is much larger than the overall scatter in the data suggesting something unusual is taking place in the error space when estimating the uncertainties in the model parameters.

In the case of P_1 and m, the uncertainties are approximately 22% and 160%, respectively. The uncertainties in the parameters P_1 and m are larger than those reported by *Kwon et al*. [2001] because of the different methods used to estimate them (*e.g.*, using a linear vs. a non-linear method). When *Kwon et al*. [2001] used a linear method, the error space was modified and two of the parameters (*e.g.*, k_0 and P_1) could not be directly calculated from the fit. The non-linear fitting method used in this study directly estimated all parameters, and has a different error space than the linearized model. Due to these differences in the way parameters are estimated by the two different methods, the uncertainties associated with each one will be different, in this case larger when using the non-linear routine [*e.g.*, *Motulsky*, 1996].

Our results agree, to some extent, with the previous results [*Kwon et al*., 2001] especially in that k_0 is the most sensitive parameter, and therefore very hard to constrain. The inability to constrain k_0 better results mainly from the lack of measurements made at effective pressures close to zero, as shown previously in a numerical experiment based on *Nelson's* [1975] permeability data. The lowest effective pressure at which a permeability measurement was made by *Kwon et al*. [2001] was 3 MPa, and clearly not low enough to increase the resolution of the model parameters.

After fitting the experimental data using the effective pressure approximation $P_e = P_d$, many questions arise from the estimates of the model parameters obtained. We could speculate about the reasons why there is such poor resolution of the model parameters, especially k_0. Sample-to-sample variations are very possible in this type of experiment due to variations in clay content and connected pore-space [*Katsube et al*., 1991; *Dewhurst et al*., 1998, 1999], and the variations can introduce systematic differences between the samples. The ability to constrain the model parameters, especially k_0, may be directly related to the absence of measurements near or at $P_e = 0$.

To better explore the effects of having a zero-pressure measurement in Wilcox shale data (or very close to it) a synthetic data set has been generated using the values k_0 = 1.2×10^{-17} m^2, P_1 = 18.3 MPa, and m = 0.154. Gaussian error was added as outlined previously using the original s.e. (1.12×10^{-20} m^2). At high effective pressures the permeability values become negative due to the large misfit (the standard error) associated with the data. Negative errors drawn at random from a Gaussian population can give rise to negative permeability values. To avoid introducing negative permeabilities in the analysis, a truncated Gaussian distribution has been used by repeating the addition of Gaussian error until a positive value of permeability was obtained. The same pressure values used by *Kwon et al*. [2001] were used for the numerical experiment. Two different synthetic data sets were used for this experiment, one with a zero-pressure permeability value, and one without it, and the results are summarized in Figure 25. A total of 30 realizations were done for each case.

The results show that the resolution of all model parameters in the case where a data point at $P_e = 0$ has been included is much better than the case where it has been removed. The parameter k_0, the most sensitive in our initial fit (Figure 24), shows a large difference with a 0.09% uncertainty when including a zero-pressure data point compared to a 400% uncertainity in the case where the zero-pressure data point was removed. Also notice that the distribution of values is different for the two cases. In the case where a data point at zero pressure was included, the distribution of values for k_0 stayed between 1.2-1.3 x10^{-17} m^2, whereas in the case with the lowest pressure at 3 MPa, the distribution of values widens (1.1-1.9 x10^{-17} m^2). Compared to the true value of 1.2x10^{-17} m^2, the average value of k_0 over the 30 trails for the case where the zero effective-pressure data point was included was also 1.2x10^{-17} m^2. For the case where the data point at $P_e = 0$ was removed the average value of k_0 was 1.4x10^{-17} m^2, and therefore still comparable to the design value.

The parameter P_1 is much better constrained than k_0, but it still shows some resolution differences between the two cases; in both cases the average value was slightly higher than the design value of 18.3 MPa (*e.g.*, 19.2 MPa for the case when including a data point at $P_e = 0$, and 19.6 MPa for the case where the data point at $P_e = 0$ was removed). The average uncertainties in P_1 differed by approximately 15% (*e.g.,* 7% uncertainty in the case a data point at zero-pressure was included, and 22% uncertainty in the case the zero-pressure data point was removed). The distribution of values is the same in both cases with a range of 15-23 MPa.

The parameter *m* displayed a large difference between the two cases, with

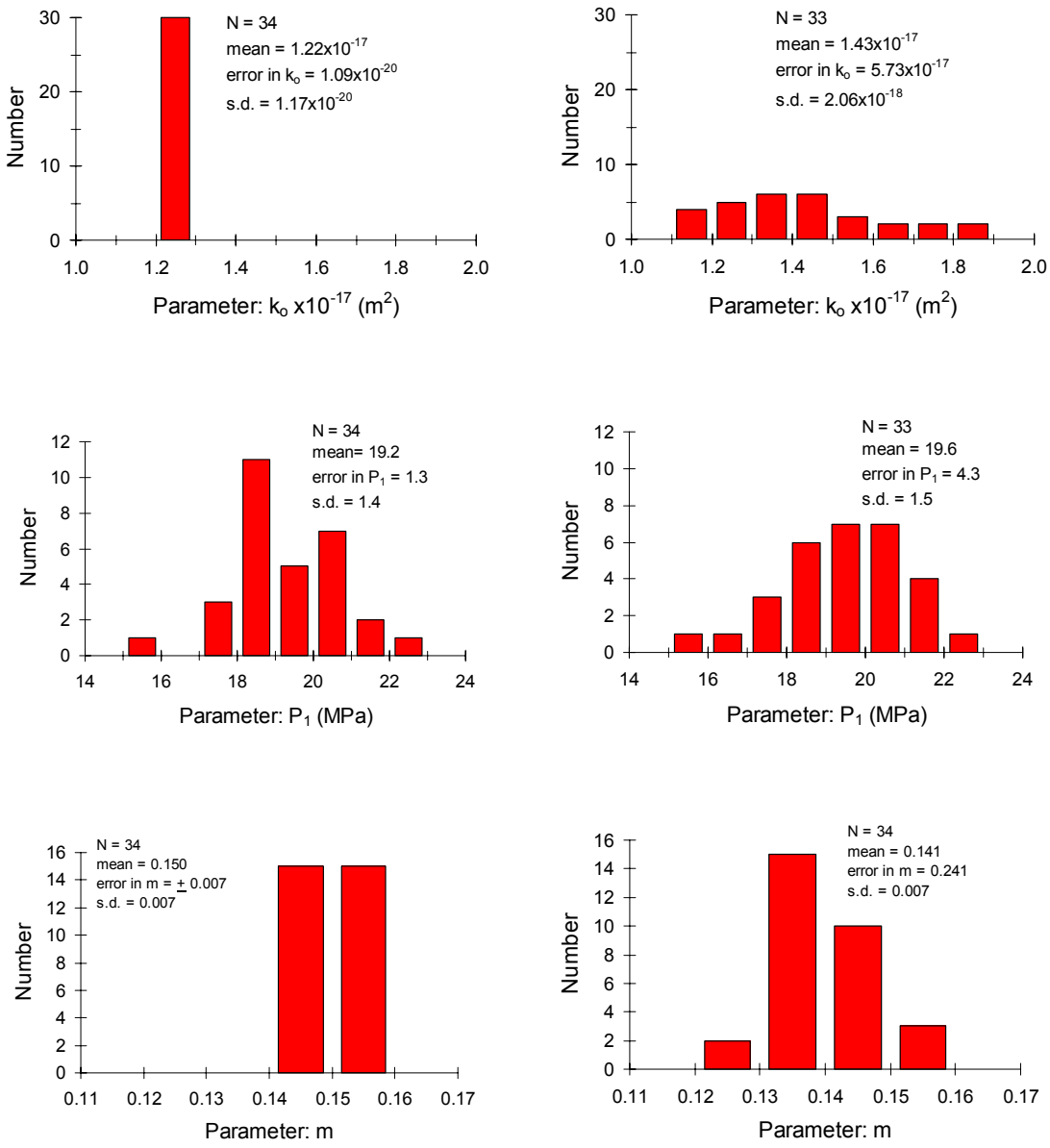

Figure 25. Histograms of parameters k_0, P_1, and m for numerical experiments based on permeability data. Left column shows case where zero-differential pressure data point has been included in the modeling, and right column shows case where zero-differential pressure data point has been removed from the modeling. N refers to the number of data points in each case. Value of error in parameter is average over 30 realizations.

uncertainties of ~5% for the case a zero-pressure data point was included, and 170% for the case with no zero-pressure data point. The case where the data point at zero-pressure was included showed a range of values for *m* of 0.14-0.16 compared to the case the data point at zero- pressure was not included with a range of 0.12-0.16.

Looking at the results from the case without a data point at $P_e = 0$ (*i.e.*, replicating the experiment by *Kwon et al*. [2001]), each trial in the modeling is consistent with the results from the experiment (Table 5). The values and uncertainties of the parameters k_0, P_1, and *m* for each trial from the numerical experiment are comparable to the values obtained from the fit to the experimental data (*i.e.,* Figure 24). The errors in all parameters, especially k_0 , are very large for the case the measurement at $P_e = 0$ was not included in the analysis.

Actually, the parameter s.e.'s from the fits should compare with the s.d. of the parameters calculated from the ensemble of 30 realizations, but in the numerical experiments without a data point at $P_e = 0$, this condition does not hold (*i.e.,* 5.8×10^{-17} m^2 and 2.1×10^{-18} m^2 for k_0, 4.3 MPa and 1.5 MPa for P_1, 0.241 and 0.007 for *m*). In the case where a measurement at $P_e = 0$ was included in the analysis, the value of the calculated uncertainties in each parameter and the s.d. of their distributions are in excellent agreement (*i.e.,* 1.1×10^{-18} m^2 and 1.2×10^{-18} m^2 in k_0, 1.3 MPa and 1.4 MPa for P_1, 0.007 and 0.007 for *m*).

We think the disagreement in the first case is because the error space is ill-conditioned due to not having a measurement at $P_e = 0$. The character of the error space

Table 5. Summary of numerical experiments based on permeability data as a function of P_c and P_p.

	CASE WITH DATA POINT AT $P_e = 0$						CASE WITHOUT DATA POINT AT $P_e = 0$					
Trial #	k_o* (m^2)	s.e.	P_l (MPa)	s.e.	m	s.e.	k_o (m^2)	s.e.	P_l (MPa)	s.e.	m	s.e.
1	1.2e-17	8.8e-21	22.3	1.4	0.141	0.005	1.1e-17	3.9e-17	22.2	5.0	0.140	0.197
2	1.2e-17	9.8e-21	19.2	1.2	0.150	0.006	1.8e-17	7.5e-17	19.5	4.0	0.129	0.217
3	1.2e-17	1.2e-20	19.7	1.6	0.147	0.007	1.6e-17	7.9e-17	19.9	5.2	0.133	0.273
4	1.2e-17	1.2e-20	18.1	1.3	0.154	0.007	1.8e-17	9.2e-17	18.4	4.4	0.132	0.265
5	1.2e-17	1.1e-20	18.2	1.3	0.154	0.007	1.6e-17	7.3e-17	18.6	4.2	0.137	0.250
6	1.2e-17	1.0e-20	19.0	1.3	0.150	0.006	1.5e-17	6.4e-17	19.2	4.2	0.138	0.238
7	1.2e-17	1.2e-20	20.0	1.6	0.146	0.007	1.7e-17	9.4e-17	20.4	5.5	0.126	0.270
8	1.2e-17	1.0e-20	18.1	1.1	0.155	0.006	1.9e-17	4.4e-17	19.8	4.5	0.145	0.265
9	1.2e-17	1.1e-20	17.6	1.2	0.158	0.007	1.5e-17	4.8e-17	20.2	4.0	0.139	0.226
10	1.2e-17	1.3e-20	20.5	1.7	0.145	0.007	1.5e-17	5.2e-17	18.8	4.2	0.148	0.256
11	1.2e-17	1.0e-20	20.9	1.4	0.142	0.006	1.4e-17	5.2e-17	17.6	3.9	0.139	0.248
12	1.2e-17	1.0e-20	20.7	1.3	0.144	0.006	1.4e-17	5.2e-17	20.8	4.5	0.138	0.216
13	1.2e-17	1.2e-20	18.4	1.4	0.153	0.007	1.3-e17	5.7e-17	21.1	5.3	0.138	0.247
14	1.2e-17	1.1e-20	18.2	1.2	0.154	0.007	1.5e-17	5.1e-17	19.7	4.6	0.139	0.237
15	1.2e-17	1.1e-20	19.4	1.4	0.147	0.007	1.3e-17	5.0e-17	19.0	5.1	0.139	0.248
16	1.2e-17	1.2e-20	18.5	1.4	0.152	0.007	1.4e-17	6.1e-17	21.5	4.9	0.146	0.234
17	1.2e-17	1.1e-20	21.1	1.6	0.141	0.006	1.3e-17	5.7e-17	21.1	5.3	0.138	0.247
18	1.2e-17	1.1e-20	19.2	1.4	0.151	0.007	1.3e-17	4.9e-17	17.6	4.0	0.138	0.249
19	1.2e-17	1.1e-20	19.0	1.3	0.151	0.007	1.4e-17	4.7e-17	18.3	3.7	0.145	0.263
20	1.2e-17	9.3e-21	17.8	1.0	0.154	0.006	1.3e-17	4.5e-17	17.9	3.4	0.152	0.221
21	1.2e-17	8.0e-21	20.7	1.1	0.145	0.004	1.1e-17	5.1e-17	20.8	3.6	0.150	0.193
22	1.2e-17	8.0e-21	20.7	1.1	0.142	0.005	1.1e-17	5.0e-17	21.0	3.8	0.148	0.248
23	1.2e-17	9.6e-21	21.5	1.4	0.141	0.005	1.3e-17	5.4e-17	19.8	5.0	0.148	0.248
24	1.2e-17	1.1e-20	18.7	1.3	0.150	0.007	1.4e-17	6.0e-17	18.8	4.3	0.143	0.255
25	1.2e-17	1.2e-20	17.3	1.3	0.158	0.008	1.2e-17	5.8e-17	21.5	4.1	0.151	0.248
26	1.2e-17	1.3e-20	18.4	1.5	0.153	0.008	1.4e-17	5.5e-17	20.8	3.8	0.136	0.238
27	1.2e-17	1.0e-20	15.5	0.9	0.159	0.007	1.7e-17	6.5e-17	15.8	2.8	0.151	0.237
28	1.2e-17	9.7e-21	19.1	1.2	0.149	0.006	1.5e-17	4.8e-17	17.0	3.7	0.140	0.238
29	1.2e-17	1.3e-20	20.5	1.7	0.144	0.008	1.2e-17	4.8e-17	19.7	4.6	0.148	0.229
30	1.2e-17	1.2e-20	18.9	1.4	0.153	0.007	1.5e-17	5.2e-17	20.4	4.0	0.149	0.240

* e = 10 to the power of

is causing it to overestimate the parameter errors in each trial, even though the standard deviations for all parameters are in excellent agreement (except for k_0, but it still behaves more like the case with a data point at zero pressure) with the ideal case when a measurement at $P_e = 0$ was included. The issue here has to do with the curvature matrix α (refer to *Bevington and Robinson* [1992]), which in the non-linear case depends directly on the sum of values of the dependent variable (*e.g.*, permeability) at the different pressures. The permeability value at $P_e = 0$ MPa is significantly larger than the next bigger value at $P_e = 3$ MPa and therefore increases the value of the curvature α. Larger values of the curvature α give rise to lower errors in the parameters. Therefore, when this data point at $P_e = 0$ is removed, the uncertainties in the parameters become much larger than expected, even though the s.e. of the fit does not significantly change from one case to another.

We also adopted a similar approach as the one shown in *Kwon et al*. [2001] where they set k_0 as a constant when fitting the Bed-of-Nails model to the permeability data to estimate the other model parameters P_1 and m. We used the same k_0 value used by *Kwon et al*. [2001] of 1×10^{-17} m^2, but applying a non-linear fit to the experimental data to determine P_1 and m. The results from this fit are shown in Figure 26.

The results from Figure 25 show that the obtained estimates of model parameters P_1 and m when setting $k_0 = 1 \times 10^{-17}$ m^2 as a constant in the non-linear fit are comparable to the results reported by *Kwon et al*. [2001] obtained using a linear approach. The estimated parameters P_1 and m for the non-linear case were 18.1 $\pm$ 1.2 MPa, and 0.167 $\pm$ 0.007, respectively, with an s.e. of 1.12×10^{-20} m^2. These values are statistically similar to

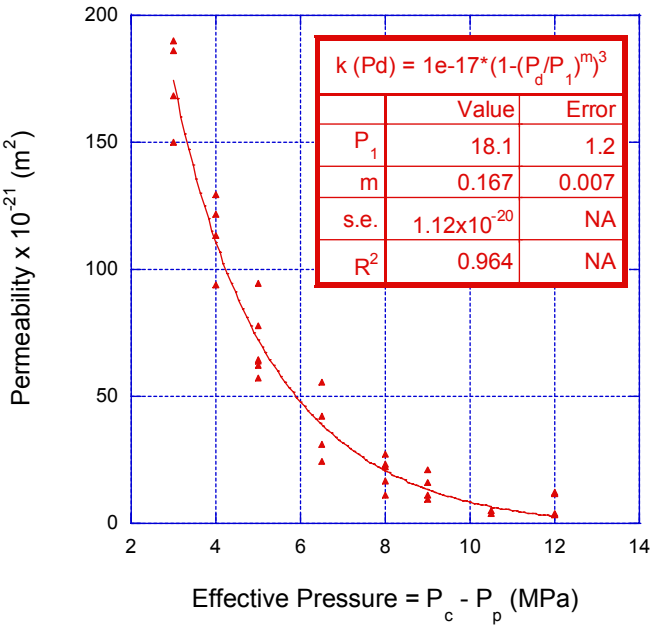

Figure 26. Best-fitting curve to permeability experimental data using k_0 = 1x10^{-17} m^2 as a constant in the fit. Values of parameters P_1 and m are determined from the fit.

the ones reported by *Kwon et al*. [2001] of 19.3 $\pm$ 1.6 MPa and 0.159 $\pm$ 0.007, with an s.e. of 1.15x10^{-20} m^2.

These results indicate that for this permeability data set, both approaches (*e.g*., linear vs. non-linear) yield valid estimates for the parameters P_1 and m when k_0 is set as a constant. Ideally, a non-linear fitting routine is preferred over the linearized version because the data itself behaves in a non-linear fashion [*Motulsky*, 1996]. Constraining k_0 is what the problem amounts to at the end, either by setting it to be a constant when fitting the data, or preferably, by having a measurement at P_e = 0, in order to better constrain the model parameters.

Lastly, we have generated error surfaces for the parameters k_0, P_1, and m as a function of χ^2 (chi-square) for two different cases: 1) the normal case without the

linearization shown by equation (17), and 2) the linearized case shown by equation (52). To illustrate how the error surfaces were generated, let us rewrite equation (26) as

$$\chi^2 = \sum \frac{\Delta_i^{\,2}}{\sigma_i^{\,2}} \tag{53}$$

where $\Delta_i^{\,2} = \left[y_i - y(x_i; \mathbf{P}^{(n)})\right]^2$.

If we assume σ_i is a constant, then we rewrite (53) as

$$\chi^2 = \frac{1}{\sigma_i^{\,2}} \sum \Delta_i^{\,2} \tag{54}$$

If we let $\sigma_i^{\,2} \approx S^2$, where S^2 is the defined as

$$S^2 = \frac{1}{N-\gamma} \sum \Delta_i^{\,2} \tag{55}$$

where S is the standard error, and $N-\gamma$ are the degrees of freedom, which for *Kwon*'s data set [*Kwon et al*., 2001] is 30. We can now rewrite (54) as

$$\chi^2 = \frac{1}{S^2} \sum \Delta_i^{\,2} \tag{56}$$

We can also define the Δ_i's for both cases as follows,

$$\Delta_i = k_i - k_o[1-(P_i/P_1)^m)^3 \qquad \text{(normal case)} \tag{57}$$

$$\Delta_i = \log[1-(k_i/k_o)^{1/3}] - m\log P_i + m\log P_1 \qquad \text{(linearized case)} \tag{58}$$

where k_i is the ith permeability value, P_i is the ith pressure value, and k_0, P_1, and m are the Bed-of-Nails model parameters.

What we have done is to vary the value of one of the parameters, keeping the other two fixed at a constant value, and calculate the value of χ^2 at the different values of the

parameter of interest using the two different approaches established in equation (57-58). The constants values we have used for the model parameters were obtained from the original non-linear fit to the data (Figure 24) of k_0, P_1, and m of 1.2×10^{-17} m^2, 18.3 MPa, and 0.154, respectively. The results are shown in Figure 27.

There are various points to make from Figure 27: 1) χ^2 is quadratic in the neighborhood of the minimum in both cases, as shown by the good fits applied, 2) the solutions for the two cases (*i.e.*, the normal case vs. the linearized case) are different, and 3) the linearized, logarithmic form yields larger error in k_0, P_1, and m compared to the "normal" form, as displayed by the more open, broader curves of the linearized case. Based on these results, we make the conclusion that in fact the error surfaces are different for the two cases previously mentioned, and at least for this particular data set the "normal" case should yield better estimates of the model parameters, given the other conditions are favorable (such as having a measurement at zero-effective pressure).

We tried fitting higher-degree effective pressure approximations (*i.e.*, those including more parameters) to the original experimental data set [*Kwon et al.*, 2001] with no success. There is no indication that a model other than the one used here fits this particular data set, and the evidence for that is the absence of systematic misfit in the original fit to the data. The large scatter in the data, as well as possible sample-to-sample variations, represents an obstacle to modeling this particular data set. Permeability measurements subject to both confining and pore-fluid pressures represent a higher challenge because of the need to constrain two different variables, as supposed to only one as in *Nelson* [1975] permeability data.

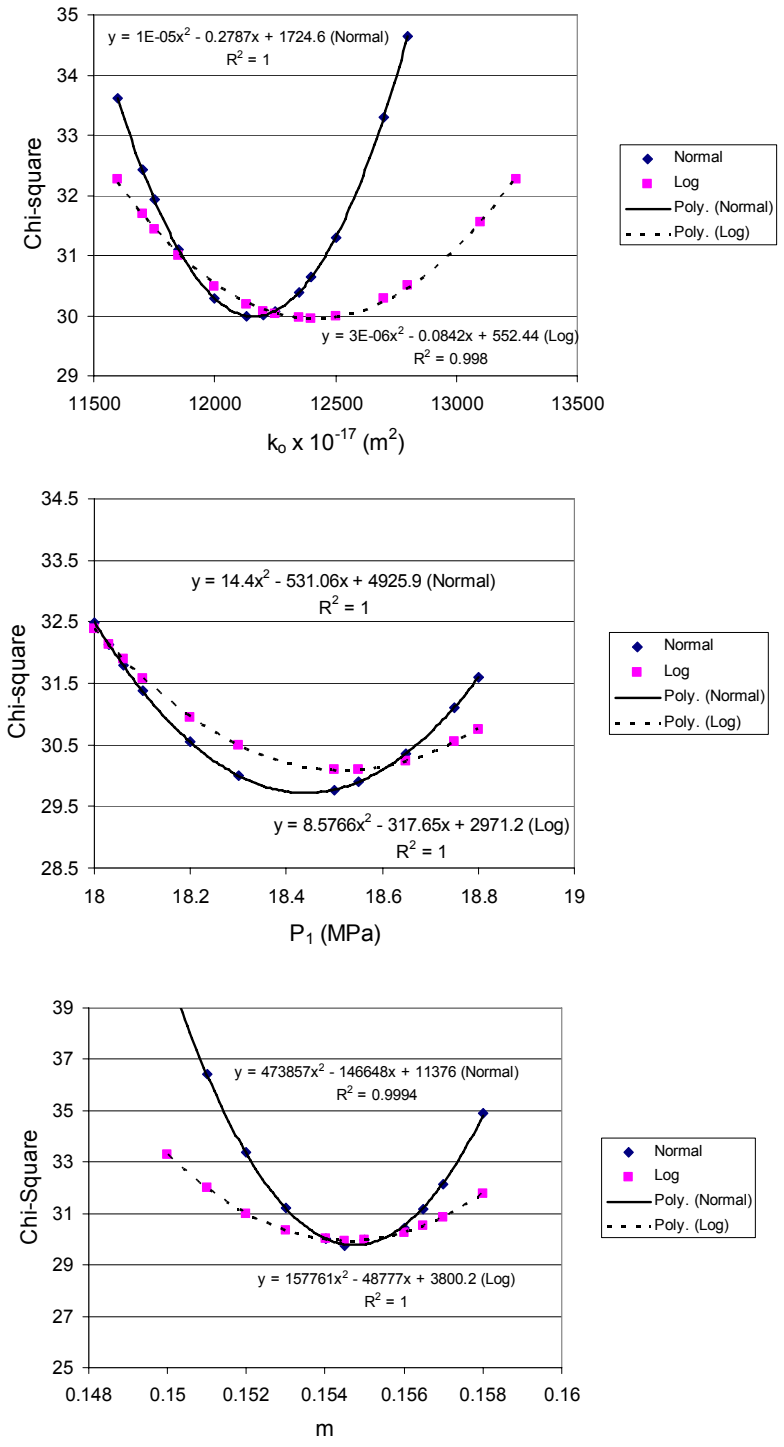

Figure 27. Error surfaces for parameters k_o, P_1, and m. Two different approaches: 1) normal, and 2) linearized. Second order polynomials have been fitted to the data, shown in solid (for "normal" case) and dashed (for linearized, logarithmic case). Equations of the fits are also indicated in each case.

The principal result of this limited experiment is that the resolution of model parameters k_0, P_1, and m is highly dependant on measurements made at $P_e = 0$ (as it was the case in *Nelson* [1975]), and lack of these measurements determines, to a great extent, our inability to constrain the models. These results have implications for experimental designs for these types of experiments where making measurements near zero-pressure may be decisive. Also, the methodology used to estimate model parameters can have a big impact on the outcome. *Kwon et al*. [2001] failed to estimate the error in k_0, and underestimated the errors in for P_1 and m. Our non-linear fitting routine did not generate as good estimates as with the linear case used by *Kwon et al*. [2001], but it directly estimated all three parameters. The linearization of (17) may not be an accurate approach because only one of the three parameters (*e.g.*, m) is directly estimated, while P_1 is being back-calculated. k_0 was only given a particular value to minimize the error in the linear fit, and therefore is only an approximation to the true value. The error space changes significantly when using the two different methods. Future experiments should carefully take into account the choice of material, the number of samples over which measurements are made, and especially measurements made at or near $P_e = 0$.

CHAPTER VIII

CONCLUSIONS

The main objective of this study was to assess the resolution of various velocity and permeability experimental data sets [*Nelson*, 1975; *Carlson and Gangi*, 1985; *Gangi and Carlson*, 1996; *Kwon et al*., 2001] using the Bed-of-Nails [*Gangi*, 1975, 1978] asperity-deformation model as the base theoretical model. These experimental sets included velocity and permeability measurements as a function of confining pressure [*Nelson*, 1975; *Carlson and Gangi*, 1985] and confining and pore-fluid pressure [*Gangi and Carlson*, 1996; *Kwon et al*., 2001]. Effective pressure approximations (equations (5-7)) were applied to each data set (except *Kwon et al*. [2001] data set where only the first definition, P_d, applied). Numerical experiments were done based on all four experimental data sets, and the results used to explore resolution issues associated with each experiment, as well as other specific issues pertinent to particular data sets and models. These results can be used to improve the design of such experiments, and therefore increase their resolution and efficiency. The following conclusions are made:

1. In most cases, the uncertainties in the model parameters are proportional to the misfit (*e.g.*, the s.e.) of the data set, at least for the compressional velocity data set [*Carlson and Gangi*, 1985] as a function of confining pressure that was used. However, this result did not apply for permeability data sets (e.g., *Nelson* [1975], *Kwon et al* [2001]) where the conditions were different compared to the velocity data. Specifically, the lack of measurements at $P_e = 0$ in the permeability data sets resulted in the error

space behaving differently (compared to the case the measurement at P_e = 0 was included), and the model parameters not being well-constrained.

2. Extrapolation of high-pressure compressional velocity measurements up to 600 MPa obtained from those made at low pressures (0-100 MPa) is acceptable, even for the case where only 9 measurements were made at the 0-100 MPa range. The error in the extrapolated values was only 1.28% for the case only 9 data points were used. The parameter that proved to be most critical when extrapolating was P_i, and its resolution decreased as less data points were used in the 0-100 MPa range. The most important condition when extrapolating is to start with a sound theoretical model that explains the data very well.

3. Measurements of compressional velocity for a deep-sea-chalk sample [*Gangi and Carlson*, 1996] over a range of confining and pore pressures have been successfully fitted using the Bed-of-Nails model [*Gangi*, 1975, 1978]. The parameter P_i proved to be most sensitive to changes in error for this velocity data set and could not be resolved when the levels of error in the data were high. We expected the P_e definitions (or approximations) to be sensitive to the scatter in the data; however, the P_e definitions were still constrained (*e.g.,* χ , χ_o , a were constrained even though P_i was not distinguishable from zero) when high levels of error were present in the data.

4. Measurements made at very low pressures are particularly important to constrain the model parameters in permeability data sets for through-going-crack permeability. In *Nelson's* [1975] permeability data set, the measurement made at P_c = 0 proved to be very important to constrain the model parameters k_0, P_1, and m. Numerical experiments

showed that P_1 is the parameter most sensitive to the zero-pressure data point. Increasing the number of measurements over the entire pressure range by a factor of 3, but still without including one at $P_c = 0$, did not significantly improve the resolution of the model parameters.

5. Model parameters in permeability data as a function of both confining and pore-fluid pressure [*e.g.*, *Kwon et al*., 2001] may be hard to resolve due to the difficulty of obtaining low-pressure measurements. The lack of low-pressure measurements, especially at $P_e = 0$, limits the ability to constrain model parameters, especially k_0, causing the error space to behave different. Because of this, k_0 must be constrained either by finding it through a grid search, or preferably having a measurement at $P_e = 0$. The specific methodology (*e.g.*, linear vs. non-linear) used to model the data is also very important because it affects how accurate the estimated uncertainties in the parameters are. When the data behaves non-linearly, it is appropriate to model it using a non-linear fitting routine. However, the linearized approach used in *Kwon et al* [2001] yielded valid estimates of the parameters and the results were comparable to the non-linear approach used in our study.

REFERENCES

Bernabe, Y. (1986), The effective pressure law for permeability in Chelmsford granite and Barre granite, *Int. J. Rock Mech. Min. Sci., 23*, 267-275.

Bernabe, Y. (1987), The effective pressure law for permeability during pore pressure and confining pressure cycling of several crystalline rocks, *J. Geophys. Res., 92*, 649-657.

Bevington, P. R. (1969), *Data Reduction and Error Analysis for the Physical Sciences*, 336 pp., McGraw-Hill, New York.

Bevington, P. R., and D. K. Robinson (1992), *Data Reduction and Error Analysis for the Physical Sciences*, 2nd ed., 336 pp., McGraw-Hill, New York.

Box, G. E. P., and M. E. Muller (1958), A note on the generation of random normal deviates, *Ann. Math. Stat., 29*, 610-611.

Brace, W. F., J. B. Walsh, and W. T. Frangos (1968), Permeability of granite under high pressure, *J. Geophys. Res., 73*, 2225-2236.

Carlson, R. L., and A. F. Gangi (1985), Effect of cracks on the pressure dependence of P wave velocities in crystalline rocks, *J. Geophys. Res., 90*, 8675-8684.

Christensen, N. I. (1974), Compressional wave velocities in possible mantle rocks to pressures of 30 kilobars, *J. Geophys. Res., 79*, 407-412.

Ciampa, J. D. (1980), Microcracks, residual strain, velocity and elastic properties of igneous rocks from a geothermal test-hole at Fenton Hill, New Mexico, M.S. Thesis, Texas A&M Univ., College Station, TX 77843.

David, C., and M. Darot (1989), Permeability and conductivity of sandstones, in *Rock at Great Depth*, edited by V. Maury and D. Foumaintraux, pp. 203-209, A. A. Balkema, Brookfield, VT.

Dewhurst, D. N., A. C. Aplin, J.-P. Sarda, and Y. Yang (1998), Compaction-driven evolution of porosity and permeability in natural mudstones: An experimental study, *J. Geophys. Res., 103*, 651-661.

Dewhurst, D. N., A. C. Aplin, J.-P. Sarda, and Y. Yang (1999), Influence of clay fraction on pore-scale properties and hydraulic conductivity of experimentally compacted mudstones, *J. Geophys. Res., 104*, 29,261-29,274.

Gangi, A. F. (1975), Variation of whole and fractured porous rock permeability with confining pressure, paper presented at First International Symposium on Induced Seismicity, Banff, Alberta, Canada.

Gangi, A. F. (1978), Variation of whole and fractured porous rock permeability with confining pressure, *Int. J. Rock Mech. Min. Sci. Geomech. Abstr., 15*, 249-257.

Gangi, A. F. (1981), The variation of mechanical and transport properties of cracked rock with pressure, *Proc. U.S. Symp. Rock Mech., 22*, 88-89.

Gangi, A. F., and R. L. Carlson (1986), An asperity-deformation model for effective pressure (abstr.), *EOS Trans. Am. Geophys. Union*, *67*, 1203.

Gangi, A. F., and R. L. Carlson (1996), An asperity-deformation model for effective pressure, *Tectonophysics*, *256*, 241-251.

Greenwood, J. A., and J. B. P Williamson (1966), Contact of nominally flat surfaces, *Proc. Roy. Soc. Lond., 295*, 300-319.

Handin, J. (1958), Effects of pore pressure on the experimental deformation of some sedimentary rocks, *Geol. Soc. Am. Bull., 69*, 1576-1577.

Hubbert, M. K., and W. W. Rubey (1959), Role of fluid pressure in mechanics of overthrust faulting, *Geol. Soc. Am. Bull., 70*, 115-166.

Jennrich, R. I., and M. L. Ralston (1979), Fitting nonlinear models to data, *Annu. Rev. Biophys. Bioeng., 8*, 195-238.

Jones, F. O. (1975), A laboratory study of the effects of confining pressure on the fracture flow and storage capacity in carbonate rocks, *J. Petrol. Technol., 21*, 21-27.

Katsube, T. J., B. S. Mudford, and M. E. Best (1991), Petrophysical characteristics of shales from the Scotian Shelf, *Geophysics*, *56*, 1681-1689.

Kwon, O., A. K. Kronenberg, A. F. Gangi, and B. Johnson (2001), Permeability of Wilcox shale and its effective pressure law, *J. Geophys. Res., 106*, 19339-19353.

Levenberg, K. (1944), A method for the solution of certain problems in least squares, *Quart. Appl. Math., 2*, 164-168.

LuValle, M. J. (2004), Some Bayesian experimental design theory for risk reduction in extrapolation, *Risk Analysis*, *24*, 1249-1259.

Marquardt, D. (1963), An algorithm for least-squares estimation of nonlinear parameters, *SIAM J. Appl. Math., 11*, 431-441.

Motulsky, H. J., and L. A. Ransnas (1987), Fitting curves to data using nonlinear regression: a practical and nonmathematical review, *FASEB J., 1*, 365-374.

Motulsky, H. J. (1996), The GraphPad Guide to Nonlinear Regression, 17 pp., GraphPad Software, San Diego.

Nelson, R. (1975), Fracture Permeability in porous reservoirs: experimental and field approach, Ph.D. Dissertation, Texas A&M Univ., College Station, TX 77843.

Nur, A., and J. D. Byerlee (1971), An exact effective stress law for elastic deformation of rock with fluids, *J. Geophys. Res., 76*, 6414-6419.

Parrish, D. K., and A. F. Gangi (1981), A nonlinear least squares technique for determining multiple-mechanism, high-temperature creep flow laws, in *Mechanical Behavior of Crustal Rocks*, *Geophys. Monogr. Ser., 24*, edited by N. L. Carter, M. Friedman, J. M. Logan, and D. W. Sterns, pp. 287-298, AGU, Washington, D. C.

Robin, P.-Y. F. (1973), Note on effective pressure, *J. Geophys. Res., 78*, 2434-2437.

Sutherland, H. J., and S. P. Cave (1980), Argon gas permeability of New Mexico rock salt under hydrostatic compression, *Int. J. Rock Mech. Min. Sci., 17*, 281-288.

Terzaghi, K. (1936), The shearing resistance of saturated soils and the angle between the planes of shear, in *Proceedings of the 1st International Conference on Soil Mechanics and Foundation Engineering*, pp. 54-56, Harvard Univ. Press, Cambridge, Mass.

Todd, T., and G. Simmons (1972), Effect of pore pressure on the velocity of compressional waves in low-porosity rocks, *J. Geophys. Res., 77*, 3731-3743.

Trimmer, D. A. (1981), Design criteria for laboratory measurements of low permeability rocks, *Geophys. Res. Lett., 8*, 973-975.

Walls, J., and A. Nur (1979), Pore pressure and confining pressure dependence of permeability in sandstone, Proceedings of the 7th Formation Evaluation Symposium of the Can. Well Logging Soc., Calgary, Alberta.

Walsh, J. B. (1981), Effect of pore pressure and confining pressure on fracture permeability, *Int. J. Rock Mech. Min. Sci., 18*, 429-435.

Walsh, J.B., and M. A. Grosenbaugh (1979), A new model for analyzing the effect of fractures on compressibility, *J. Geophys*. *Res*., *84*, 3532-3536.

Wilhelmi, B., and W. H. Somerton (1969), Simultaneous measurement of pore and elastic properties of rocks under triaxial stress conditions, *Soc*. *Petrol*. *Engin*. *Jour*., *7*, 283-294.

Wolf, A. V., M. G. Brown, and P. G. Prentiss (1979), Concentrative properties of aqueous solutions: Conversion tables, in *CRC Handbook of Chemistry and Physics*, 60th ed., edited by R. C. Weast, pp. D227-D276, CRC Press, Boca Raton, FL.

APPENDIX 1

Table A-1. Epidote data summary

P_c (MPa)	V_p (km/s)	P_c (MPa)	V_p (km/s)
1.4	6.628	280.0	7.378
2.8	6.653	300.0	7.393
3.4	6.681	320.0	7.407
4.1	6.695	340.0	7.418
5.5	6.726	360.0	7.433
6.9	6.740	380.0	7.442
8.3	6.755	400.0	7.456
10.0	6.781	420.0	7.465
13.8	6.803	440.0	7.471
20.0	6.849	460.0	7.479
24.1	6.839	500.0	7.488
30.0	6.864		
34.5	6.896		
37.9	6.926		
41.4	6.946		
44.8	6.964		
48.3	6.977		
50.0	6.987		
55.2	7.005		
60.0	7.025		
62.1	7.033		
65.5	7.041		
69.0	7.051		
72.4	7.062		
75.9	7.091		
79.3	7.101		
82.8	7.114		
86.2	7.125		
100.0	7.162		
110.0	7.184		
120.0	7.203		
130.0	7.217		
140.0	7.227		
160.0	7.266		
180.0	7.288		
200.0	7.302		
220.0	7.313		
240.0	7.336		
260.0	7.364		

VITA

Ezequiel Genova Barazarte received his Bachelor of Science degree in marine geology from Eckerd College in St. Petersburg, FL in May 2003. He entered the geophysics program at Texas A&M University in College Station, TX in August 2004, and he received his Master of Science degree in August 2007. His research interests include petroleum geology and geophysics.

Mr. Genova Barazarte will start working at Marathon Oil Company following his graduation, as a geologist in the Gulf of Mexico Asset Team. He can be reached at Marathon Oil Company, 5555 San Felipe, Houston, TX., 77056. His email address is ezequiel.genova@gmail.com.